SKB

TECHNICAL REPORT 92-05

Buoyancy flow in fractured rock with a salt gradient in the groundwater – An initial study

Johan Claesson

Department of Building Physics, Lund University, Sweden

February 1992

SVENSK KÄRNBRÄNSLEHANTERING AB
SWEDISH NUCLEAR FUEL AND WASTE MANAGEMENT CO

BOX 5864 S-102 48 STOCKHOLM

TEL 08-665 28 00 TELEX 13108 SKB S
TELEFAX 08-661 57 19

BUOYANCY FLOW IN FRACTURED ROCK WITH A SALT GRADIENT IN THE GROUNDWATER - AN INITIAL STUDY

Johan Claesson

Department of Building Physics, Lund University, Sweden

February 1992

BUOYANCY FLOW IN FRACTURED ROCK WITH A SALT GRADIENT IN THE GROUNDWATER

-An initial study

JOHAN CLAESSON

February 1992

Study for Swedish Nuclear Fuel and Waste Management Co.

Dept. of Building Physics, Lund University, Sweden

Foreword

This study is made for the Swedish Nuclear Fuel and Waste Management Co (SKB). I have had good discussions and advice from the experts of SKB. The computer model is developed by Johan Bennet. My co-worker Göran Hellström has also contributed to the work.

Johan Claesson

Dept. of Building Physics, Lund University, Sweden

Abstract

Nuclear waste, deposited in canisters in rock, produces heat that will induce a buoyancy flow of groundwater in fractures. The radioactive material may then, in case of leakage, possibly reach the biosphere. The groundwater density will increase downwards with an increasing salt content. This density increase counteracts the thermal buoyancy, and it may create a natural barrier for the repository.

The aim of the study is to analyse this barrier effect and to assess the extent of upward flow. The coupled flow process for groundwater, salt and heat is studied. The equations have been analysed in great detail, and a numerical model has been developed for the case of groundwater flow in a fracture or crack plane.

The largest upward motion from the repository has been determined with the model for a wide range of heat release. Approximate formulas, which are shown to be sufficiently accurate for assessments, have been derived.

There is a very clear barrier effect. In a reference case with a salt concentration increase of 2% per km downwards, and with as much as 300 canisters (releasing all in all 0.32 TWh) placed in a limited region, the largest upward movement of groundwater from the repository region became 150 m. The result is remarkably insensitive to variations of the involved parameters (heat release, distance from canisters to fracture plane, considered time, salt concentration gradient, thermal expansivity, hydraulic conductivity of flow plane and so on).

Contents

Chapter 1

Introduction

Nuclear waste, deposited in canisters in rock, produces heat that will induce a buoyancy flow of groundwater in fractures. The radioactive material may then, in case of leakage, eventually reach the biosphere.

There is often a significant increase downwards of the salt concentration of the groundwater. This means that the water density increases downwards. The density increase will counteract the thermal buoyancy. This may create a natural barrier that prevents the groundwater of the nuclear waste region ever to reach the ground surface.

These ideas from SKB are presented in Juhlin and Sandstedt (1989). Hodgkinson (1980) presents an investigation of thermally induced convection without any salt gradients.

This study, which is a first step, is made in order to investigate the idea of a salt gradient barrier and to try to assess how far below the ground surface the store must be placed for any given salt gradient. Other important questions are the limits on heat release and the best way to place the canisters under different restraints.

The report contains quite a lot of different analyses that may require some time to digest. Therefore, there is a rather detailed survey of the line of thought and the main results in the last chapter. The reader is adviced to read Chaper 7 first.

Chapter 2

Governing equations

The governing equations for the coupled flow problem are discussed in this chapter. A general reference for flow in porous media is Bear (1972).

2.1 Equations for water, salt and heat

The mass balance equation for the groundwater reads:

$$\frac{\partial}{\partial t}(V_p \rho_w) + \nabla \cdot (\rho_w \vec{q}_w) = 0 \tag{2.1}$$

We start in this chapter with the case when the ground is treated as a *homogeneous, isotropic porous medium.* The volumetric groundwater flow is then given by Darcy's law:

$$\vec{q}_w = -\frac{k}{\mu_w}(\nabla P + g\rho_w \hat{z}) \tag{2.2}$$

There is a corresponding balance equation for the salt:

$$\frac{\partial}{\partial t}(cV_p \rho_w) + \nabla \cdot (c\rho_w \vec{q}_w) = 0 \tag{2.3}$$

The second term concerns the convective salt flow $c\rho_w \vec{q}_w$. We have here neglected dispersive (and diffusive) flow of salt.

Finally, there is a heat balance equation, which determines the temperature:

$$\frac{1}{a}\frac{\partial T}{\partial t} = \frac{\partial^2 T}{\partial x^2} + \frac{\partial^2 T}{\partial y^2} + \frac{\partial^2 T}{\partial z^2} + \frac{h(x,y,z,t)}{\lambda} = \nabla^2 T + \frac{h}{\lambda} \tag{2.4}$$

Here, h denotes the prescribed heat sources. The ground is assumed to be thermally homogeneous. The convective heat flow $(c_w(T - T_{ref}) \cdot \rho_w \vec{q}_w)$ is neglected. This is a very reasonable approximation, since we are dealing with very small groundwater flows.

The following notations are used in the above equations:

t	time	(s)
V_p	pore volume	(m_w^3/m^3)
ρ_w	density of water	(kg/m^3)
$\nabla = \left(\frac{\partial}{\partial x}, \frac{\partial}{\partial y}, \frac{\partial}{\partial z}\right)$	gradient operator	(m^{-1})
$\vec{q}_w = (q_{wx}, q_{wy}, q_{wz})$	volumetric groundwater flow	(m_w^3/m^2s)
k	intrinsic permeability	(m^2)
μ_w	dynamic viscosity of water	(kg/ms)
P	water pressure	(Pa)
$g = 9.81$	standard gravity	(m/s^2)
$\hat{z}$	vertical unit vector pointing upwards	(-)
c	salt concentration	(kg_s/kg_w)
a	thermal diffusivity of the ground	(m^2/s)
T	temperature	(°C)
x, y	horizontal coordinates	(m)
z	vertical coordinate pointing upwards	(m)
λ	thermal conductivity of the ground	(W/mK)

Here, m_w^3 denotes cubic meter of water, kg_s kilogram of dissolved salt and kg_w kilogram of water including the dissolved salt.

The properties of water depend on its state. In general, the density ρ_w and the viscosity μ_w are functions of T, c, and P. The buoyancy force $-g\rho_w\hat{z}$ in the Darcy law will change when T and c change. The groundwater flow is coupled to the time-varying temperature and salt distributions.

2.2 Independent thermal process

The thermal process, Eq. (2.4), depends on the heat sources, but it is independent of the groundwater flow and the salt distribution. This is due to the fact that the convective heat flow can be neglected in the present applications. The *uncoupled* thermal processes can be solved independently. The temperature field $T(x, y, z, t)$ is from this solution a given function in the remaining problem for groundwater and salt.

The initial temperature is given by the undisturbed ground temperature T_o, or $T_o(z)$ with an increase downwards according to the geothermal gradient:

$$T|_{t=0} = T_o(z) \tag{2.5}$$

The canisters are located far below the ground surface. The influence from the conditions at the ground surface can then be neglected.

Let $T''(x, y, z, t)$ denote the deviation from the undisturbed ground temperature:

$$T(x, y, z, t) = T''(x, y, z, t) + T_o(z) \tag{2.6}$$

The initial condition and the boundary condition far away from the depository in all directions for the *excess* temperature T'' become:

$$T''|_{t=0} = 0 \qquad T''|_{\text{infinity}} = 0 \tag{2.7}$$

A dimensionless temperature T' will also be used. Let T_1 be a suitable temperature level from the heating caused by the heat sources $h(x, y, z, t)$. The *dimensionless excess temperature* T' is given by:

$$T'' = T_1 \cdot T' \qquad T = T_o(z) + T_1 \cdot T' \tag{2.8}$$

2.3 Further assumptions. Basic equations

We will make a few further assumptions for the groundwater and salt flow process. We use Boussinesq's approximation in which the groundwater density is taken constant in all terms except in the buoyancy term $g\rho_w\hat{z}$:

$$\rho_w = \rho_{wo} \quad \text{except in} \quad g\rho_w\hat{z} = g\rho_w(T, c)\hat{z} \tag{2.9}$$

In the buoyancy term, the density is a function of temperature and salt concentration. The dependence on the pressure P can be neglected in the present applications.

Equation (2.3) for salt mass balance can now be written (since ρ_w and the porosity V_p are constant):

$$\frac{\partial c}{\partial t} + \nabla \cdot (c\vec{v}_f) = 0 \tag{2.10}$$

The salt with the concentration c is displaced with the *filtration velocity* $\vec{v}_f$ (m/s):

$$\vec{v}_f = \frac{1}{V_p}\vec{q}_w \tag{2.11}$$

The velocity $\vec{v}_f$ is obtained from Darcy's law (2.2):

$$\vec{v}_f = -\frac{k}{V_p\mu_w}[\nabla P + g\rho_w(T, c)\hat{z}] \tag{2.12}$$

The divergence of $\vec{v}_f$ is, according to Eq. (2.1) with $V_p\rho_w$ constant, zero:

$$\nabla \cdot \vec{v}_f = \frac{\partial v_{fx}}{\partial x} + \frac{\partial v_{fy}}{\partial y} + \frac{\partial v_{fz}}{\partial z} = 0 \tag{2.13}$$

The viscosity μ_w depends on T and c. See Section 3.5. The present applications concern temperatures from 10 to 100°C, in which range the viscosity varies by a factor 4.6. The larger variations concern a rather limited region near the heat sources. Our main interest is, however, the behaviour at larger distances.

We will use a constant value for the viscosity:

$$\mu_w = \mu_{wo} \tag{2.14}$$

With this crucial assumption, the factor $k/(V_p\mu_w)$ in (2.12) becomes constant, and we will be able to use *analytical expressions* for the groundwater flow. Then we get from (2.12-13) the following equation to determine the pressure $P(x, y, z, t)$:

$$\nabla^2 P + g\frac{\partial \rho_w}{\partial z} = 0 \tag{2.15}$$

This is a Poisson equation with the source term given by the derivative of $\rho_w(T, c)$ with respect to z:

$$\frac{\partial \rho_w}{\partial z} = \left(\frac{\partial \rho_w}{\partial T}\right)_c \cdot \frac{\partial T}{\partial z} + \left(\frac{\partial \rho_w}{\partial c}\right)_T \cdot \frac{\partial c}{\partial z} \tag{2.16}$$

The equations for the groundwater pressure and the salt concentration are now:

$$\begin{aligned} &\nabla^2 P + g\frac{\partial \rho_w}{\partial z} = 0 \qquad \rho_w = \rho_w(T, c) \\ &\frac{\partial c}{\partial t} + \nabla \cdot (c\vec{v}_f) = 0 \\ &\vec{v}_f = -\frac{k}{V_p\mu_{wo}}(\nabla P + g\rho_w \hat{z}) \end{aligned} \tag{2.17}$$

We have the following alternative forms for the first two equations:

$$\nabla \cdot \vec{v}_f = 0 \qquad \frac{\partial c}{\partial t} + \vec{v}_f \cdot \nabla c = 0 \tag{2.18}$$

The temperature $T(x, y, z, t)$ is obtained independently. See Section 2.2.

The initial concentration at $t = 0$ is equal to the undisturbed value $c_o(z)$:

$$c|_{t=0} = c_o(z) \tag{2.19}$$

The concentration $c_o(z)$ increases downwards: $dc_o/dz \leq 0$.

The ground surface, lying far above the active flow region, is neglected, and we treat the ground as infinite in all directions. The flow tends to zero as the distance to the depository tends to infinity:

$$\vec{v}_f \to \vec{0} \qquad \sqrt{x^2 + y^2 + z^2} \to \infty \tag{2.20}$$

The complete problem involves the three functions $T(x, y, z, t)$, $P(x, y, z, t)$, and $c(x, y, z, t)$. Expressed explicitly in these functions, the equations become:

$$\begin{aligned} &\frac{1}{a}\frac{\partial T}{\partial t} = \nabla^2 T + \frac{h}{\lambda} \\ &\nabla^2 P + g\frac{\partial \rho_w}{\partial T} \cdot \frac{\partial T}{\partial z} + g\frac{\partial \rho_w}{\partial c} \cdot \frac{\partial c}{\partial z} = 0 \end{aligned}$$

$$\frac{\partial c}{\partial t} - \frac{k}{V_p \mu_{wo}} \nabla \cdot \{c\,[\nabla P + g\rho_w(T,c)\hat{z}]\} = 0 \tag{2.21}$$

$$T|_{t=o} = T_o(z) \qquad c|_{t=o} = c_o(z)$$

The main assumptions in the above formulation are:

1. The ground is a homogeneous, isotropic porous medium.
2. The water viscosity μ_w is constant.
3. Salt dispersion and diffusion are neglected.

There are a few other assumptions, which are judged to be very well satisfied in the present applications:

4. Convective heat transfer is negligible.
5. Boussinesq's approximation, using constant ρ_w except in the buoyancy term, is valid.

2.4 Deviation from equilibrium

The process starts with heat release from $t = 0$. There is an equilibrium state before this time:

$$t < 0: \qquad T = T_o(z) \quad c = c_o(z) \quad \left(\frac{dc_o}{dz} \leq 0\right)$$

$$\rho_w = \rho_w\left(T_o(z), c_o(z)\right) = \rho_w^o(z) \tag{2.22}$$

For the hydrostatic pressure $P_o(z)$ we have according to Eq. (2.15):

$$\frac{d^2 P_o}{dz^2} + g\frac{d\rho_w^o}{dz} = 0$$

$$P_o(z) = P_o(z_o) - g\int_{z_o}^{z} \rho_w^o(z')dz' \tag{2.23}$$

In equilibrium with negligible regional flow, the groundwater flow is of course zero:

$$\nabla P_o(z) = -g\rho_w^o(z)\hat{z} \quad \Longleftrightarrow \quad \vec{v}_{fo} = \vec{0} \tag{2.24}$$

We will in the following consider the deviations from equilibrium. These *excess* variables are denoted T'', c'' and P'':

$$T(x,y,z,t) = T_o(z) + T''(x,y,z,t)$$

$$c(x,y,x,t) = c_o(z) + c''(x,y,z,t) \tag{2.25}$$

$$P(x,y,z,t) = P_o(z) + P''(x,y,z,t)$$

The groundwater flow is driven by the excess density ρ'':

$$\rho'' = \rho_w\left(T_o(z) + T'', c_o(z) + c''\right) - \rho_w\left(T_o(z), c_o(0)\right) \tag{2.26}$$

We get from the difference between Eqs. (2.15) and (2.23):

$$\nabla^2 P'' + g\frac{\partial \rho''}{\partial z} = 0 \tag{2.27}$$

The flow $\vec{v}_f$ depends, in accordance with Eqs. (2.12) and (2.24), on the excess variables only:

$$\vec{v}_f = -\frac{k}{V_p \mu_{wo}}\left(\nabla P'' + g\rho''\hat{z}\right) \tag{2.28}$$

The basic equations for the deviations from initial equilibrium are now:

$$\nabla^2 P'' + g\frac{\partial \rho''}{\partial z} = 0 \qquad \rho'' = \rho_w\left(T_o(z) + T'', c_o(z) + c''\right) - \rho_w\left(T_o(z), c_o(z)\right)$$

$$\frac{\partial c''}{\partial t} + \nabla \cdot \left[(c_o(z) + c'')\vec{v}_f\right] = 0$$

$$\vec{v}_f = -\frac{k}{V_p \mu_{wo}}\left(\nabla P'' + g\rho''\hat{z}\right) \tag{2.29}$$

$$c''|_{t=0} = 0$$

All excess variables tend to zero at infinity. It should be noted that the groundwater flow involves the excess variables only, while the convective salt flow involves the total salt concentration $c_o(z) + c''$.

2.5 Linearized water density

The water density ρ_w depends on the temperature T and the salt concentration c. The partial derivatives define the thermal expansion coefficient α_T (1/K) and a corresponding coefficient α_c (1/(kg$_s$/kg$_w$)) for the relative density increase with the salt concentration c:

$$\left(\frac{\partial \rho_w}{\partial T}\right)_c = -\rho_{wo}\alpha_T \qquad \left(\frac{\partial \rho_w}{\partial c}\right)_T = \rho_{wo}\alpha_c \tag{2.30}$$

We now assume that these two coefficients are *constants*. Then the excess density ρ'' becomes a simple linear function of c'' and T'', Eq.(2.26):

$$\rho'' = \rho_{wo}\alpha_c c'' - \rho_{wo}\alpha_T T'' \tag{2.31}$$

The basic equations (2.17) or (2.29) for P'' and c'' now become:

$$\begin{aligned}
&\nabla^2 P'' + g\rho_{wo}\alpha_c \frac{\partial c''}{\partial z} - g\rho_{wo}\alpha_T \frac{\partial T''}{\partial z} = 0 \\
&\frac{\partial c''}{\partial t} + \nabla \cdot [(c_o(z) + c'')\vec{v}_f] = 0 \\
&\vec{v}_f = -\frac{k}{V_p \mu_{wo}} (\nabla P'' + g\rho_{wo}\alpha_c c''\hat{z} - g\rho_{wo}\alpha_T T''\hat{z})
\end{aligned} \tag{2.32}$$

The temperature T'' is determined independently. The initial value of c'' at $t = 0$ is zero.

The second equation may in accordance with Eq. (2.18) be written in the alternative form:

$$\frac{\partial c''}{\partial t} + \vec{v}_f \cdot \left(\frac{dc_o}{dz}\hat{z} + \nabla c'' \right) = 0 \tag{2.33}$$

2.6 Dimensionless formulation

It is quite convenient to use a dimensionless formulation. A length L_1, a time t_1, and so on, are used:

Length L_1:	x/L_1, ... dimensionless coordinates
	$L_1\nabla$ dimensionless gradient
Time t_1:	$t_1\partial/\partial t$ dimensionless time derivative
Pressure P_1:	$P' = P''/P_1$ dimensionless excess pressure
Temperature T_1:	$T' = T''/T_1$ dimensionless excess temperature
Concentration c_1:	$c' = c''/c_1$ dimensionless excess concentration
Velocity v_{f1}:	$\vec{v}_f = \vec{v}_f/v_{f1}$ dimensionless filtration velocity

The first equation of (2.32) becomes in a dimensionless form:

$$L_1^2\nabla^2 P' + \frac{g\rho_{wo}\alpha_c c_1 L_1}{P_1} \cdot \left(L_1 \frac{\partial c'}{\partial z} - \frac{\alpha_T T_1}{\alpha_c c_1} L_1 \frac{\partial T'}{\partial z} \right) = 0 \tag{2.34}$$

For the second equation of (2.32) we use the alternative form (2.33). The dimensionless form becomes:

$$t_1 \frac{\partial c'}{\partial t} + \frac{t_1}{L_1}\vec{v}_f \cdot \left(\frac{dc_o}{dz}\frac{L_1}{c_1}\hat{z} + L_1\nabla c' \right) = 0 \tag{2.35}$$

For the filtration velocity we get, using the last equation (2.32):

$$\frac{t_1}{L_1}\vec{v}_f = -\frac{t_1}{L_1} \cdot \frac{k}{V_p\mu_{wo}} \cdot \frac{P_1}{L_1} \left[L_1\nabla P' + \frac{g\rho_{wo}\alpha_c c_1 L_1}{P_1} \left(c' - \frac{\alpha_T T_1}{\alpha_c c_1} T' \right) \hat{z} \right] \tag{2.36}$$

The above equations give directly a natural choice for the scale factors L_1, t_1 and so on.

We assume for simplicity that the undisturbed salt gradient is *constant*:

$$-\frac{dc_o}{dz} = c_z^o = \text{constant} \tag{2.37}$$

In accordance with equation (2.35), we choose:

$$c_1 = c_z^o L_1 \tag{2.38}$$

The factor before $\hat{z}$ is then -1. The constant c_1 is positive, since the gradient $dc_o/dz = -c_z^o$ must be negative. Then the water density increases downwards and the salt stratification is stable. (Actually, stability requires that $\rho_w^o(z)$, Eq.(2.22), increases downwards.) The concentration c_1 is equal to the undisturbed concentration difference over the height L_1.

The pressure factor P_1 is in accordance with Eqs. (2.34) and (2.36) chosen as:

$$P_1 = g\rho_{wo}\alpha_c c_1 L_1 \tag{2.39}$$

Physically, this is the excess pressure from the salt with the concentration c_1 over the characteristic height L_1.

The scale factor t_1 for time is determined in the following way. The second and third factors on the righthand side of (2.36) give a characteristic filtration velocity:

$$v_{f1} = \frac{k}{V_p\mu_{wo}} \cdot \frac{P_1}{L_1} = \frac{kg\rho_{wo}\alpha_c c_1}{V_p\mu_{wo}} \tag{2.40}$$

Here, P_1/L_1 is a characteristic pressure gradient. The time t_1 is now chosen as:

$$\frac{t_1}{L_1} \cdot v_{f1} = 1$$

or, with $t_1 = t_c$:

$$t_c = \frac{L_1}{v_{f1}} = \frac{V_p\mu_{wo}}{kg\rho_{wo}\alpha_c c_z^o} \tag{2.41}$$

We use the particular notation t_c for this *characteristic* time-scale. It is a fundamental quantity. It is important to note that t_c is determined by the groundwater flow parameters and the salt gradient only. It does not depend on the length L_1 and the thermal process.

The length L_1 is still free. It may be chosen so that the factor before T' in (2.36) and (2.34) vanishes:

$$\alpha_T T_1 = \alpha_c c_1 \tag{2.42}$$

or with (2.38):

$$L_1 = \frac{\alpha_T T_1}{\alpha_c c_z^o} \tag{2.43}$$

The quantity $\alpha_T T_1$ is the relative density change when the water temperature is increased T_1 °C, while $\alpha_c c_1$ is the relative density change for a concentration change c_1. The length L_1 is chosen so that $\alpha_c c_1$ equals $\alpha_T T_1$, which means that the two density variations become of the same order.

With these choices, the flow equations (2.34-36) become:

$$\begin{aligned} L_1^2 \nabla^2 P' + L_1 \frac{\partial c'}{\partial z} - L_1 \frac{\partial T'}{\partial z} &= 0 \\ t_c \frac{\partial c'}{\partial t} + \vec{v}_f' \cdot (-\hat{z} + L_1 \nabla c') &= 0 \\ \vec{v}_f' &= -L_1 \nabla P' - c' \hat{z} + T' \hat{z} \end{aligned} \tag{2.44}$$

The first equation means that $\nabla \cdot \vec{v}_f' = 0$. The second equation may then be written in the original form:

$$t_c \frac{\partial c'}{\partial t} + L_1 \nabla \cdot \left[\left(-\frac{z}{L_1} + c' \right) \vec{v}_f' \right] = 0 \tag{2.45}$$

This means that the dimensionless undisturbed salt distribution is $-z/L_1$; i.e. there is a unit gradient in the length scale L_1.

2.7 Summary of equations

We will here summarize the complete set of equations. The coordinates are scaled with the length L_1, and the time with the characteristic time t_c:

$$x' = x/L_1 \quad y' = y/L_1 \quad z' = z/L_1 \qquad t' = t/t_c$$

The temperature T, pressure P, salt concentration c and filtration velocity $\vec{v}_f$ are scaled in the following way:

$$\begin{aligned} T(x,y,z,t) &= T_o(z) + T_1 \cdot T'(x',y',z',t') \\ P(x,y,z,t) &= P_o(z) + P_1 \cdot P'(x',y',z',t') \\ c(x,y,z,t) &= c_o(z) + c_1 \cdot c'(x',y',z',t') \\ \vec{v}_f(x,y,z,t) &= v_{f1} \cdot \vec{v}_f'(x',y',z',t') \end{aligned} \tag{2.46}$$

The following constants are used:

$$L_1 = \frac{\alpha_T T_1}{\alpha_c c_z^o} \qquad t_c = \frac{V_p \mu_{wo}}{k g \rho_{wo} \alpha_c c_z^o} \qquad c_1 = c_z^o L_1$$

$$P_1 = g\rho_{wo}\alpha_c c_1 L_1 \qquad v_{f1} = \frac{L_1}{t_c} \tag{2.47}$$

The temperature field T or T' is determined independently of the other processes by the prescribed heat sources. The temperature factor T_1 or the length L_1 may be chosen freely.

The dimensionless equations for pressure, salt concentration and filtration flow are:

$$(\nabla')^2 P' + \frac{\partial c'}{\partial z'} - \frac{\partial T'}{\partial z'} = 0 \tag{2.48}$$

$$\frac{\partial c'}{\partial t'} + \nabla' \cdot \left[(-z' + c')\vec{v}_f'\right] = 0 \tag{2.49}$$

$$\vec{v}_f' = -\nabla' P' - c'\hat{z} + T'\hat{z} \tag{2.50}$$

$$c'|_{t=0} = 0 \qquad T' \text{ given independently} \tag{2.51}$$

All variables vanish at infinity. The solution is a function of the dimensionless coordinates and the dimensionless time. It is noteworthy that the equations do not contain *any* intrinsic parameters. A number of parameters will, however, arise from the temperature field.

The dimensionless total salt concentration is given by $-z' + c'$. We will use a special notation:

$$\tilde{c} = -z' + c' \tag{2.52}$$

Equation (2.49) may then be written:

$$\frac{\partial \tilde{c}}{\partial t'} + \nabla' \cdot (\tilde{c}\,\vec{v}_f') = 0 \tag{2.53}$$

We have the following alternative form for Eqs. (2.48) and (2.49):

$$\nabla' \cdot \vec{v}_f' = 0 \tag{2.54}$$

$$\frac{\partial c'}{\partial t'} + (-\hat{z} + \nabla' c') \cdot \vec{v}_f' = 0 \tag{2.55}$$

The index $'$ is cumbersome. We will sometimes in the following drop it. The basic equations (2.48-2.51) then read:

$$\nabla^2 P + \frac{\partial c}{\partial z} - \frac{\partial T}{\partial z} = 0$$

$$\frac{\partial c}{\partial t} + \nabla \cdot [(-z + c)\vec{v}_f] = 0 \tag{2.56}$$

$$\vec{v}_f = -\nabla P - c\hat{z} + T\hat{z}$$

$$c|_{t=0} = 0 \qquad T \text{ given independently}$$

Chapter 3

Water flow in a plane

Chapter 2 dealt with three-dimensional flow in a homogeneous porous medium. We now limit the groundwater flow to two-dimensional flow in a plane. The plane may be a fracture zone, which is essentially limited to a plane. It may also be a single fracture or a number of (interconnected) parallel fractures.

The flow plane is assumed to be infinite: $y = 0, -\infty < x < \infty, -\infty < z < \infty$. The ground surface is assumed to lie far above the region of interest so that the boundary conditions can be ignored. The flow and salt variables $P, \vec{v}_f$ and c are functions of x, z and t. The temperature field is of course three-dimensional, but we are only interested in the temperature $T(x, 0, z, t)$ in the flow plane $y = 0$.

In this two-dimensional case, the radial distance from the center is:

$$r = \sqrt{x^2 + z^2} \tag{3.1}$$

3.1 Governing equations

Let $\vec{q}^c$ denote the volumetric groundwater flow integrated over the width of the fracture zone. Its dimension is m^3 of water/(m·s). Darcy's law (2.2) for the flow in a *vertical* plane reads:

$$\vec{q}^c = -\frac{k^c}{\mu_w}(\nabla P + g\rho_w \hat{z}) \tag{3.2}$$

Here, k^c is the intrinsic hydraulic conductivity for the fracture zone.

The Darcy equation above refers to the case of a vertical plane with the gravity force $g\rho_w\hat{z}$. This force is reduced by the factor $\cos(\phi_c)$ when the plane is inclined an angle ϕ_c to the vertical line. We will in the following give the equations for a vertical plane. The gravity g is to be replaced by $g\cos(\phi_c)$, if the plane is inclined.

The filtration velocity (2.11-12) is obtained by dividing $\vec{q}^c$ by the water volume V_p^c ($m^3_w/m^2_{\text{fracture}}$). Eq. (2.12) becomes:

$$\vec{v}_f = -\frac{k^c}{V_p^c \mu_w}(\nabla P + g\rho_w \hat{z}) \tag{3.3}$$

In the two-dimensional case, we shall replace k/V_p by k^c/V_p^c.

The fracture zone may sometimes be regarded as a homogeneous porous medium with a width B. Then we have:

$$k^c = Bk \qquad V_p^c = BV_p \quad \Longrightarrow \quad \frac{k^c}{V_p^c} = \frac{k}{V_p} \tag{3.4}$$

Another idealized case is a number N_c of parallel cracks, each having the constant width d. We assume laminar flow. Then from Poiseuille's law we have:

$$\vec{q}^c = N_c \cdot (-)\frac{d^3}{12\mu_w}(\nabla P + g\rho_w \hat{z}) \tag{3.5}$$

This gives:

$$k^c = \frac{N_c d^3}{12} \qquad V_p^c = N_c \cdot d \tag{3.6}$$

Thus, for parallel planes, each with the width d, we have:

$$\frac{k^c}{V_p^c} = \frac{d^2}{12} \tag{3.7}$$

It is interesting to note that this quantity is independent of the number of planes.

Thus, the final equations in Section 2.7 are also applicable in the two-dimensional case. The y-coordinate vanishes. The quantity k/V_p is replaced by k^c/V_p^c or $d^2/12$. For an inclined plane g is replaced by $g\cos(\phi_c)$.

3.2 Flow for any density distribution $\rho''(x,z)$

The excess density ρ'' due to excess temperature and salt concentration is for any particular time a function of the coordinates: $\rho'' = \rho''(x,z)$. As a prerequisite for further studies, we will here study the pressure and flow fields for any density distribution.

The excess density ρ'' may with the use of (2.31) and (2.42) be written:

$$\rho'' = \rho_{wo}\alpha_c c_1(c' - 1 \cdot T') = \rho_{wo}\alpha_c c_1 \cdot \rho'$$
$$\rho' = c' - T' \tag{3.8}$$

We use the *dimensionless* equations (2.56), in which the indices $'$ and $''$ are *dropped.* We have with $c' - T' = \rho' \rightarrow \rho$:

$$\nabla^2 P + \frac{\partial \rho}{\partial z} = 0 \tag{3.9}$$

$$\vec{v}_f = -\nabla P - \rho\hat{z} \tag{3.10}$$

The variables P, ρ and $\vec{v}_f$ are functions of x and z (for any particular time t). By assumption, the excess density $\rho(x,z)$ vanishes sufficiently rapidly for large radius r. We require in the case of a radial density variation $\rho = \rho(r)$:

$$\int_1^\infty \ln(r)\rho(r) r\, dr \qquad \text{convergent} \tag{3.11}$$

3.2.1 General solution

The Poisson problem (3.9) has the well-known integral solution, Courant and Hilbert (1968):

$$P(x,z) = -\frac{1}{4\pi}\int_{-\infty}^{\infty} dx' \int_{-\infty}^{\infty} dz' \cdot \ln\left[(x'-x)^2 + (z'-z)^2\right] \cdot \frac{\partial \rho(x',z')}{\partial z'} \tag{3.12}$$

The velocity field is obtained directly by derivation:

$$v_{fx} = -\frac{\partial P}{\partial x} = -\frac{1}{2\pi}\int_{-\infty}^{\infty} dx' \int_{-\infty}^{\infty} dz' \frac{x'-x}{(x'-x)^2 + (z'-z)^2} \frac{\partial \rho(x',z')}{\partial z'} \tag{3.13}$$

$$v_{fz} = -\frac{\partial P}{\partial z} - \rho = -\frac{1}{2\pi}\int_{-\infty}^{\infty} dx' \int_{-\infty}^{\infty} dz' \frac{z'-z}{(x'-x)^2 + (z'-z)^2} \frac{\partial \rho(x',z')}{\partial z'} - \rho(x,z)$$

The source term of the Poisson equation is the derivative of ρ with respect to z. Let $U(x,z)$ be the solution for the source term $\rho(x,y)$:

$$\nabla^2 U + \rho = 0 \tag{3.14}$$

The pressure $P(x,z)$ is then the derivative of $U(x,z)$ with respect to z:

$$P(x,z) = \frac{\partial U}{\partial z} \tag{3.15}$$

The solution of (3.14), for a density that tends to zero sufficiently rapidly, is:

$$U(x,z) = -\frac{1}{4\pi}\int_{-\infty}^{\infty} dx' \int_{-\infty}^{\infty} dz' \cdot \ln\left[(x'-x)^2 + (z'-z)^2\right] \cdot \rho(x',z') \tag{3.16}$$

It is straightforward to verify by partial integration that (3.15) and (3.16) give (3.12).

3.2.2 General solution for $\rho = \rho(r)$

The temperature field from a single heat source at a point $(0, y_o, 0)$ will become rotationally symmetric: $T(x,0,z,t) = f(r,t)$. This means that the corresponding density depends on r only (at any particular time t). The case $\rho = \rho(r)$ is therefore quite important in the present applications.

In this case $\rho = \rho(r)$, we start with the equation for U:

$$\nabla^2 U + \rho(r) = 0 \tag{3.17}$$

The solution $U(r)$ depends on r only. In radial coordinates we have:

$$\frac{1}{r}\frac{d}{dr}\left(r\frac{dU}{dr}\right) + \rho(r) = 0 \tag{3.18}$$

The solution is obtained by two integrations:

$$U(r) = A + B \cdot \ln(r) - \int_0^r \frac{1}{r''} \left[\int_0^{r''} r' \rho(r') dr' \right] dr'' \tag{3.19}$$

We require that U is regular at $r = 0$. The integration constant B must be zero. The derivative of U becomes:

$$\frac{dU}{dr} = -\frac{1}{r} \int_0^r r' \rho(r') dr' \tag{3.20}$$

For the pressure $P(x, z)$ we get:

$$P(x,z) = \left(\frac{\partial U(r)}{\partial z} \right)_x = \frac{dU}{dr} \cdot \left(\frac{\partial r}{\partial z} \right)_x = \frac{dU}{dr} \cdot \frac{z}{r} \tag{3.21}$$

This gives the pressure:

$$P(x,z) = -\frac{z}{x^2 + z^2} \cdot \int_0^r r' \rho(r') dr' \qquad r = \sqrt{x^2 + z^2} \tag{3.22}$$

The corresponding flow field $\vec{v}_f$ is obtained from the gradient of P, Eq. (3.10). The flow field may after a few rearrangements be written in the following, quite illuminating way:

$$v_{fx} = \frac{2xz}{(x^2 + z^2)^2} \cdot f_\rho(r) \tag{3.23}$$

$$v_{fz} = -\frac{x^2 - z^2}{(x^2 + z^2)^2} \cdot f_\rho(r) - \frac{\rho}{2} \tag{3.24}$$

The radial function $f_\rho(r)$ is given by:

$$f_\rho(r) = \frac{r^2}{2} \rho(r) - \int_0^r r' \cdot \rho(r') dr' = \frac{1}{2} \int_0^r (r')^2 \frac{d\rho}{dr'} dr' \tag{3.25}$$

3.2.3 Dipole field

The first factors of v_{fx} and v_{fz} give a so-called *dipole field.* Let us investigate this. Consider the pressure field:

$$P(x,z) = \frac{z}{x^2 + z^2} = \frac{\partial}{\partial z} \left[\ln \left(\sqrt{x^2 + z^2} \right) \right] \tag{3.26}$$

This field has a dipole singularity at $(0,0)$. The corresponding flow field becomes:

$$v_{fx} = -\frac{\partial P}{\partial x} = \frac{2xz}{(x^2 + z^2)^2} \qquad ((x,z) \neq (0,0)) \tag{3.27}$$

$$v_{fz} = -\frac{\partial P}{\partial z} = -\frac{x^2 - z^2}{(x^2 + z^2)^2} \tag{3.28}$$

The isobars of (3.26) becomes:

$$P = \frac{z}{x^2 + z^2} \qquad x^2 + z^2 - \frac{z}{P} = 0 \tag{3.29}$$

or

$$x^2 + \left(z - \frac{1}{2P}\right)^2 = \frac{1}{4P^2} \tag{3.30}$$

This is the equation for a circle with radius $1/|2P|$ and the center at $(0, 1/(2P))$. The isobars are circles which all have the x-axis as tangent at $(0,0)$. The flow field will follow orthogonal curves. These are circles with the z-axis as tangent at $(0,0)$. The situation is illustrated in Figure 3.1.

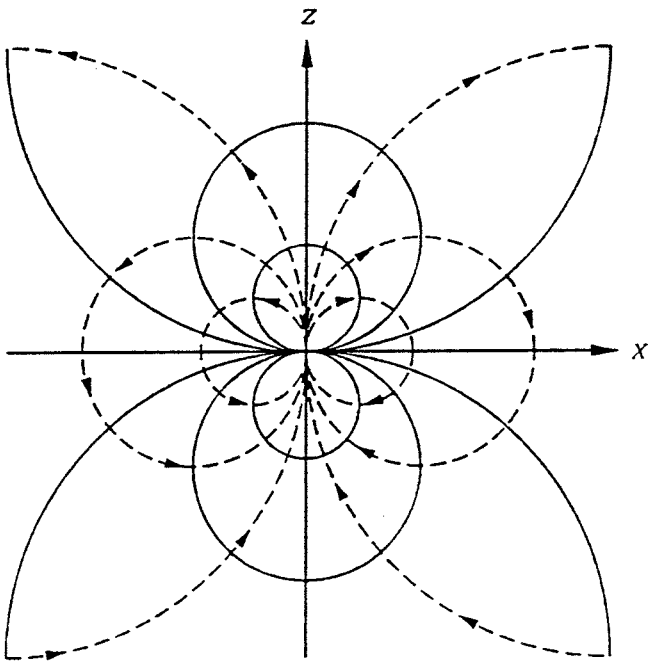

Figure 3.1. Isobars (full lines) and flow lines (dashed) for the dipole field.

3.2.4 Two examples

As a first example for the above formulas we consider the case with a *warmer circular region*:

$$\rho(r) = \begin{cases} -\rho_1 & 0 \le r < r_1 \\ 0 & r > r_1 \end{cases} \tag{3.31}$$

Then we have:

$$r < r_1 : f_\rho(r) = \frac{r^2}{2}(-\rho_1) - \int_0^r r'(-\rho_1)dr' = 0$$

$$v_{fx} = 0 \qquad v_{fz} = \frac{\rho_1}{2} \tag{3.32}$$

$$r > r_1 : f_\rho(r) = 0 - \int_0^{r_1} r'(-\rho_1)dr' = \frac{\rho_1 r_1^2}{2} = \frac{\rho_1 \pi r_1^2}{2\pi}$$

$$v_{fx} = \frac{2xz}{y^2+z^2} \cdot \frac{\rho_1 \pi r_1^2}{2\pi} \qquad v_{fz} = -\frac{x^2-z^2}{(x^2+z^2)^2} \cdot \frac{\rho_1 \pi r_1^2}{2\pi} \tag{3.33}$$

We get the dipole field outside the circle $r = r_1$. It may be noted that the strength is $(\rho_1 \pi r_1^2)/(2\pi)$. The dipole strength is equal to the total weight $\rho_1 \cdot \pi r_1^2$ divided by 2π. The flow field inside the circle $r = r_1$ is constant, $\rho_1/2$, and directed upwards.

As a second example we consider the following density distribution:

$$\rho(r) = -\rho_1 e^{-r^2/r_1^2} \tag{3.34}$$

Then we get:

$$f_\rho(r) = -\frac{r^2\rho_1}{2}e^{-r^2/r_1^2} + \rho_1 \int_0^r r' e^{-(r')^2/r_1^2} dr' = \frac{\rho_1 r_1^2}{2}\left[1 - \left(1 + \frac{r^2}{r_1^2}\right) e^{-r^2/r_1^2}\right] \tag{3.35}$$

The function within the brackets behaves as $\frac{1}{2}(r/r_1)^4$ near $r = 0$, and it increases towards $+1$ for large r/r_1.

The velocity field induced by the density (3.34) is according to (3.23-25):

$$v_{fx} = \frac{2xzr_1^2}{(x^2+z^2)^2} \cdot \frac{\rho_1}{2}\left[1 - \left(1 + \frac{r^2}{r_1}\right) e^{-r^2/r_1^2}\right]$$

$$v_{fz} = -\frac{(x^2-z^2)r_1^2}{(x^2+z^2)^2} \cdot \frac{\rho_1}{2}\left[1 - \left(1 + \frac{r^2}{r_1^2}\right) e^{-r^2/r_1^2}\right] + \frac{\rho_1}{2} e^{-r^2/r_1^2} \tag{3.36}$$

3.3 Temperature and salt components

The dimensionless excess density ρ' consists of the salt concentration and temperature components, Eq.(3.8):

$$\rho' = c' - T' \tag{3.37}$$

Dropping the indices we have in accordance with (3.9,10):

$$\nabla^2 P + \frac{\partial c}{\partial z} - \frac{\partial T}{\partial z} = 0$$

$$\vec{v}_f = -\nabla P - c\hat{z} + T\hat{z} \tag{3.38}$$

We get two components for pressure and flow :

$$P = P_T + P_c \qquad \vec{v}_f = \vec{v}_T + \vec{v}_c \tag{3.39}$$

For the temperature component we have:

$$\nabla^2 P_T - \frac{\partial T}{\partial z} = 0$$

$$\vec{v}_T = -\nabla P_T + T\hat{z} \tag{3.40}$$

The salt component is determined by the equations:

$$\nabla^2 P_c + \frac{\partial c}{\partial z} = 0 \tag{3.41}$$

$$\vec{v}_c = -\nabla P_c - c\hat{z} \tag{3.42}$$

3.4 Dimensionless problem

Our final two-dimensional problem concerns an infinite plane $-\infty < x < \infty$, $-\infty < z < \infty$. The temperature field $T(x, 0, z, t)$ in the plane is obtained independently from the prescribed heat sources.

The dimensionless groundwater flow process consists of two components. The component from the temperature field is according to (3.40):

$$\nabla^2 P_T - \frac{\partial T}{\partial z} = 0 \qquad \vec{v}_T = -\nabla P_T + T\hat{z} \tag{3.43}$$

The flow field $\vec{v}_T$ is determined from the results in section 3.2 and in particular 3.2.2, and the temperature fields of Chapter 4. The flow field driven by salt concentration is the solution of:

$$\nabla^2 P_c + \frac{\partial c}{\partial z} = 0 \qquad \vec{v}_c = -\nabla P_c - c\hat{z} \tag{3.44}$$

Finally, the temporal variation of the salt concentration is determined by:

$$\frac{\partial c}{\partial t} + \nabla \cdot [(-z + c)(\vec{v}_c + \vec{v}_T)] = 0$$

$$c|_{t=0} = 0 \tag{3.45}$$

The total concentration is in the present dimensionless formulation with a linear undisturbed concentration gradient given by (2.52):

$$\tilde{c} = -z + c \tag{3.46}$$

Here, the undisturbed linear concentration, $-z$, has unit slope. The equations (3.45) may be written:

$$\frac{\partial \tilde{c}}{\partial t} + \nabla \cdot [\tilde{c}\,(\vec{v}_T + \vec{v}_c)] = 0 \quad \Longleftrightarrow \quad \frac{D(\tilde{c})}{Dt} = 0 \tag{3.47}$$

$$\tilde{c}|_{t=0} = -z$$

This equation means that the material derivative $D(\tilde{c})/Dt$ is zero. A 'salt particle' p that follows the flow $\vec{v}_T + \vec{v}_c$ does not change its concentration:

$$\tilde{c}_p(t) = \tilde{c}_p(0) = -z_p|_{t=0} \tag{3.48}$$

3.5 Physical data

The reference water density is

$$\rho_{wo} = 1000 \text{ kg/m}^3$$

The dynamic viscosity of pure water at ordinary pressure varies strongly with the temperature. We have from Smith (1979):

T (°C)	0	10	20	30	40	50	70	100
$10^6\mu_w(T)$ (kg/ms)	1790	1310	1000	798	654	547	403	282

The dependency on pressure is quite small. The viscosity increases by 1%, when the pressure is increased from $P = 1$ bar to $P = 100$ bar, Smith 1979.

The water contains salt with the concentration c ($\text{kg}_{\text{salt}}/\text{kg}_{\text{solution}}$). We use values for a solution of sodium chloride, NaCl. From CRC Handbook (1971) we have for the relative variation the dynamic viscosity with c:

c (kg_s/kg_w)	0	0.01	0.02	0.05	0.10	0.15	0.20
$\mu_w(c)/\mu_w(0)$	1	1.018	1.034	1.083	1.191	1.349	1.554

We see that the variation of viscosity with c is rather modest.

In our models we use a constant value μ_{wo} for the dynamic viscosity. As a reference value we will use:

$$\mu_{wo} = 0.7 \cdot 10^{-3} \text{ kg/ms} \tag{3.49}$$

The water density ρ_w varies with the temperature T and the concentration c. The derivatives give the thermal expansivity α_T (1/K) and a corresponding coefficient α_c ($1/(\text{kg}_s/\text{kg}_w)$) for the relative density increase with c. We have from (2.30):

$$\alpha_T = -\frac{1}{\rho_w}\left(\frac{\partial \rho_w}{\partial T}\right)_c \qquad \alpha_c = \frac{1}{\rho_w}\left(\frac{\partial \rho_w}{\partial c}\right)_T \tag{3.50}$$

The thermal expansivity α_T depends strongly on the temperature. From CRC Handbook (1971) we have for ordinary water:

T (°C)	4	10	15	20	25	30	40	50	60	70	80	90	100
$10^6\alpha_T$ (1/°C)	0	88	151	207	257	303	385	458	523	584	641	696	750

For $T = 20$°C we have as a reference value:

$$\alpha_T = 2 \cdot 10^{-4} \text{ 1/K} \tag{3.51}$$

The variation of density with c is given in CRC Handbook (1971) for many salts. For a sodium-chloride solution we have:

c (kg_s/kg_w)	0	0.01	0.03	0.05	0.1	0.15	0.20
$\rho_w(c)/\rho_w(0)$	1	1.0071	1.0214	1.0358	1.0726	1.1105	1.1498
α_c ($1/(\text{kg}_s/\text{kg}_w)$)	0.71	0.71	0.72	0.73	0.75	0.77	0.81

As a reference value we choose:

$$\alpha_c = 0.72 \quad 1/(\text{kg}_s/\text{kg}_w) \tag{3.52}$$

For granite rock we use the following thermal data:

$$\lambda = 3.5 \text{ W/mK} \qquad C = 2.16 \cdot 10^6 \text{ J/m}^3\text{K} \qquad a = \frac{\lambda}{C} = 1.62 \cdot 10^{-6} \text{ m}^2/\text{s} \tag{3.53}$$

The salt gradient $c_z^0 = -dc/dz$ is an important parameter. As reference case we take an increase of 2% for 1000 m:

$$c_z^o = \frac{0.02}{1000} = 2 \cdot 10^{-5} \quad \text{kg}_s/\text{kg}_w\text{m} \tag{3.54}$$

As a *reference case* we have the following data:

$$\begin{aligned} &\rho_{wo} = 1000 \text{ kg/m}^3 \qquad \mu_{wo} = 0.7 \cdot 10^{-3} \text{ kg/ms} \\ &\alpha_T = 2 \cdot 10^{-4} \text{ 1/K} \quad \alpha_c = 0.72 \text{ 1/(kg}_s\text{/kg}_w\text{)} \\ &\lambda = 3.5 \text{ W/mK} \quad C = 2.16 \cdot 10^6 \text{ J/m}^3\text{K} \quad a = 1.62 \cdot 10^{-6} \text{ m}^2/\text{s} \\ &c_z^o = 2 \cdot 10^{-5} \text{ kg}_s/\text{kg}_w\text{m} \end{aligned} \tag{3.55}$$

3.6 Characteristic time-scale t_c

The characteristic time-scale t_c, (2.41), is a quantity of major importance. Let d be the characteristic fracture width. Then we have from (3.7), (3.4) and (2.41):

$$t_c = \frac{12\mu_{wo}}{d^2 g \rho_{wo} \alpha_c c_z^o} \tag{3.56}$$

With the data (3.55) of the reference case we get for fracture width $d = 0.1$ and 1 mm:

$$d = 1 \text{ mm}: \quad t_c = \frac{12 \cdot 0.7 \cdot 10^{-3}}{(0.001)^2 \cdot 9.81 \cdot 1000 \cdot 0.72 \cdot 2 \cdot 10^{-5}} = 16.5 \text{ hours} \tag{3.57}$$

$$d = 0.1 \text{ mm}: \quad t_c = 1650 \text{ h} \ = 69 \text{ days} \tag{3.58}$$

It is interesting to compare this with the characteristic time-scale t_T of the variations of the temperature fields. Consider for example the continuous point source of Section 4.1.2. There is a heat release at $(0, y_o, 0)$ from $t = 0$. The temperature of the fracture plane $y = 0$ is given by (4.10). The time dependence at a distance $r = \sqrt{x^2 + z^2}$ is of the type:

$$T^c \propto \text{ erfc}(\sqrt{t_T/t}) \tag{3.59}$$

Here, erfc( ) is the complementary error function. We get from (4.10) the characteristic time-scale:

$$t_T = \frac{r^2 + y_o^2}{4a} = \frac{x^2 + y_o^2 + z^2}{4a} \tag{3.60}$$

Here, a (m^2/s) is the thermal diffusivity.

Numerically we have for example:

$$\sqrt{r^2 + y_o^2} = 100 \text{ m} \quad a = 1.62 \cdot 10^{-6} \text{ m}^2/\text{s} \quad \Rightarrow \quad t_T = 49 \text{ years} \tag{3.61}$$

So at distances *not too close* to the canisters we have that the characteristic salt-flow time t_c is much smaller than the time-scale t_T of temperature variations:

$$t_c << t_T \tag{3.62}$$

This means that the *temperature field* is *quasi-stationary* compared to the flow induced by salt variations.

Chapter 4

Temperature fields

The temperature $T(x,y,z,t)$ satisfies the heat conduction equation (2.4):

$$\frac{1}{a}\frac{\partial T}{\partial t} = \nabla^2 T + \frac{h}{\lambda} \tag{4.1}$$

Here h denotes the prescribed heat sources. We are interested in the temperature T^c in the fracture plane $y = 0$:

$$T^c(x,z,t) = T(x,0,z,t) - T_o(z) \tag{4.2}$$

The undisturbed, initial temperature $T_o(z)$ is subtracted. We will also be interested in the total weight of the warm region, i.e. the integral T^c_{int} of T^c over the plane:

$$T^c_{\text{int}}(t) = \int_{-\infty}^{\infty} dx \int_{-\infty}^{\infty} dz \cdot T^c(x,z,t) \tag{4.3}$$

4.1 Point source solutions

The heat sources are essentially, on the length scale of interest here, point sources at the canisters.

4.1.1 Instantaneous point source

A basic case is the instantaneous release of heat at a point. The heat E_o (J) is released at the point $(0, y_o, 0)$ at $t = 0$. The well-known solution (for zero initial temperature) is, Carslaw (1959):

$$T(x,y,z,t) = \frac{E_o}{C(4\pi a t)^{3/2}} e^{-\left[x^2+(y-y_o)^2+z^2\right]/(4at)} \tag{4.4}$$

Here $C = \lambda/a$ (J/m^{3}K) is the volumetric heat capacity.

The temperature in the flow plane $y = 0$ becomes:

$$T^c(x,z,t) = \frac{E_o}{C(4\pi at)^{3/2}} e^{y_0^2/(4at)} \cdot e^{-r^2/(4at)} \qquad r^2 = x^2 + z^2 \tag{4.5}$$

The integration in x and z is straightforward. We use the well-known integral:

$$\frac{1}{\sqrt{4\pi at}} \int_{-\infty}^{\infty} e^{-x^2/(4at)} dx = 1 \tag{4.6}$$

Then we get directly:

$$T^c_{\text{int}}(t) = \frac{E_o}{C\sqrt{4\pi at}} e^{-y_o^2/(4at)} \tag{4.7}$$

4.1.2 Continuous point source

Our next case concerns the continuous release of heat Q_o (W) at the point $(0, y_o, 0)$ from $t = 0$. The temperature is, by superposition, obtained from an integral of (4.4) for $0 \le t' \le t$. The heat E_o is replaced by $Q_o dt'$, and the solution (4.4) is for this contribution taken at the time $t - t'$:

$$T(x,y,z,t) = \int_0^t \frac{Q_o}{C\,[4\pi a(t-t')]^{3/2}} \cdot e^{-\left[x^2+(y-y_o)^2+z^2\right]/[4a(t-t')]}\, dt' \tag{4.8}$$

This gives with a suitable change of integration variable the well-known solution, Carslaw (1959):

$$T(x,y,z,t) = \frac{Q_o}{4\pi\lambda} \frac{1}{\sqrt{x^2+(y-y_o)^2+z^2}} \cdot \text{erfc}\left(\frac{\sqrt{x^2+(y-y_o)^2+z^2}}{\sqrt{4at}}\right) \tag{4.9}$$

Here, erfc denotes the complementary error function.

The temperature in the flow plane becomes:

$$T^c(x,z,t) = \frac{Q_o}{4\pi\lambda} \frac{1}{\sqrt{r^2+y_o^2}} \text{erfc}\left(\frac{\sqrt{r^2+y_o^2}}{\sqrt{4at}}\right) \qquad r^2 = x^2 + z^2 \tag{4.10}$$

4.1.3 Exponentially decaying point source

The heat release from the nuclear reactions in the canisters decays exponentially with a time constant t_d. We have the following heat source:

$$Q_o \cdot e^{-t/t_d} \quad \text{(W)} \quad \text{at } (0, y_o, 0) \text{ from } t = 0 \tag{4.11}$$

We get an integral of the type (4.8) where $Q_o dt'$ is replaced by $Q_o e^{-t'/t_d} dt'$:

$$T(x,y,z,t) = \int_0^t \frac{Q_o e^{-t'/t_d}}{C\,[4\pi a(t-t')]^{3/2}} e^{-\tilde{r}^2/[4a(t-t')]}\, dt' \tag{4.12}$$

$$\tilde{r}^2 = x^2 + (y-y_o)^2 + z^2$$

With the substitution $u = \tilde{r}/\sqrt{4a(t-t')}$ we get:

$$T(x,y,z,t) = \frac{Q_o}{4\pi\lambda}\frac{1}{\tilde{r}} e^{-t/t_d} \frac{2}{\sqrt{\pi}} \int_{\tilde{r}/\sqrt{4at}}^{\infty} e^{-u^2 + (\tilde{r})^2/(4at_d u^2)}\, du \tag{4.13}$$

The temperature in the fracture plane becomes:

$$T^c(x,z,t) = \frac{Q_o}{4\pi\lambda}\frac{1}{\sqrt{r^2+y_o^2}} e^{-t/t_d} \frac{2}{\sqrt{\pi}} \int_{\sqrt{r^2+y_o^2}/\sqrt{4at}}^{\infty} e^{-u^2 + (r^2+y_o^2)/(4at_d u^2)}\, du \tag{4.14}$$

For $t_d = \infty$ we regain (4.10).

4.1.4 Superposition

With the above solutions we can obtain the temperature field from any distribution of point sources. We can also add components with different decay times t_d.

4.2 Flow field for a point source

We are in particular interested in the groundwater flow field $\vec{v}_T$ induced by the temperature field. The general solution for a radially symmetric density $\rho = \rho(r)$ is given in section 3.2.2. The formulas may be applied directly for the temperature fields in the previous section.

We will here consider the simplest case with an *instantaneous point source*. The temperature in the fracture zone is from (4.5):

$$T^c(r,t) = \frac{E_o}{C(4\pi a t)^{3/2}} e^{-y_o^2/(4at)} \cdot e^{-r^2/(4at)} + T_o(z) \tag{4.15}$$

Here, we have added the undisturbed temperature $T_o(z)$. From $T^c = T_1 \cdot T' + T_o(z)$, (2.46), we get the dimensionless excess temperature T':

$$T' = \frac{E_o}{T_1 C(4\pi at)^{3/2}} e^{-y_o^2/(4at)} \cdot e^{-(r')^2 \cdot L_1^2/(4at)} \tag{4.16}$$

We do not specify T_1 or L_1. The corresponding dimensionless density $\rho' = -T'$ is of the type (3.34) with ρ_1 and r_1^2 given by:

$$\rho_1 = \frac{E_o}{T_1 C(4\pi at)^{3/2}} e^{-y_o^2/(4at)} \tag{4.17}$$

$$r_1^2 = \frac{4at}{L_1^2} \tag{4.18}$$

The flow field $\vec{v}_T$ is now given by the expressions (3.36).

The use of an *instantaneous* point source is not valid during a first period, when the exponential decay of heat release is significant. But the temperature field has a certain finite range during this period. A suitable measure of this range is, in accordance with (3.60), $\sqrt{4at_d}$. For simplicity, we will assume that the distance y_o from the flow plane to the canister region exceeds this initial range:

$$y_o > \sqrt{4at_d} \tag{4.19}$$

This means that we can use the solution (4.15) *at all times* at the flow plane $y = 0$.

Chapter 5

Numerical model

We use the *dimensionless* formulation of Section 3.4. All indices are omitted. The total dimensionless concentration $\tilde{c}(x,z,t)$ satisfies the equations (3.47):

$$\frac{\partial \tilde{c}}{\partial t} + \nabla \cdot [\tilde{c}\,(\vec{v}_T + \vec{v}_c] = 0 \tag{5.1}$$

$$\tilde{c}|_{t=0} = -z \tag{5.2}$$

The temperature-induced velocity field $\vec{v}_T$ is given by analytical expressions. The salt-induced velocity field $\vec{v}_c$ is determined by the excess concentration c. We have from (3.44), (3.9) and (3.13):

$$\vec{v}_c(x,z,t) = -c(x,z,t)\hat{z} - \frac{1}{2\pi}\int_{-\infty}^{\infty} dx' \int_{-\infty}^{\infty} dz' \frac{(x'-x, z'-z)}{(x'-x)^2 + (z'-z')^2} \cdot \frac{\partial c(x',z',t)}{\partial z'}$$

$$c = \tilde{c} + z \tag{5.3}$$

5.1 Moving salt particles

The $\tilde{c}$-curves are at the beginning $t = 0$ just straight horizontal lines in the (x,z)-plane: $\tilde{c}(x,z,0) = -z$. Curves for constant $\tilde{c}$ at a later time is shown in figure 5.1 for a typical case with heating in the center region. The flow is here directed upwards, while it becomes directed downwards further out on both sides.

The field $\tilde{c}(x,z,t)$ will be represented numerically by a number of moving particles, which follow the total flow $\vec{v}_T + \vec{v}_c$. Particle i,j has the coordinates

$$(x_{ij}(t), z_{ij}(t)) \tag{5.4}$$

At $t = 0$, the particles lie in a rectangular mesh with the coordinates (x_i, z_j) $(x_1 < x_2 < ..., z_1 < z_2 < ...)$:

$$x_{ij}(0) = x_i \qquad z_{ij}(0) = z_j \tag{5.5}$$

The particles i, j preserve according to Eq. (3.47) their initial total concentrations:

$$\tilde{c}_{ij}(t) = \tilde{c}_{ij}(0) = -z_{ij}(0) + c_{ij}(0) \tag{5.6}$$

or

$$\tilde{c}_{ij}(t) = -z_j \tag{5.7}$$

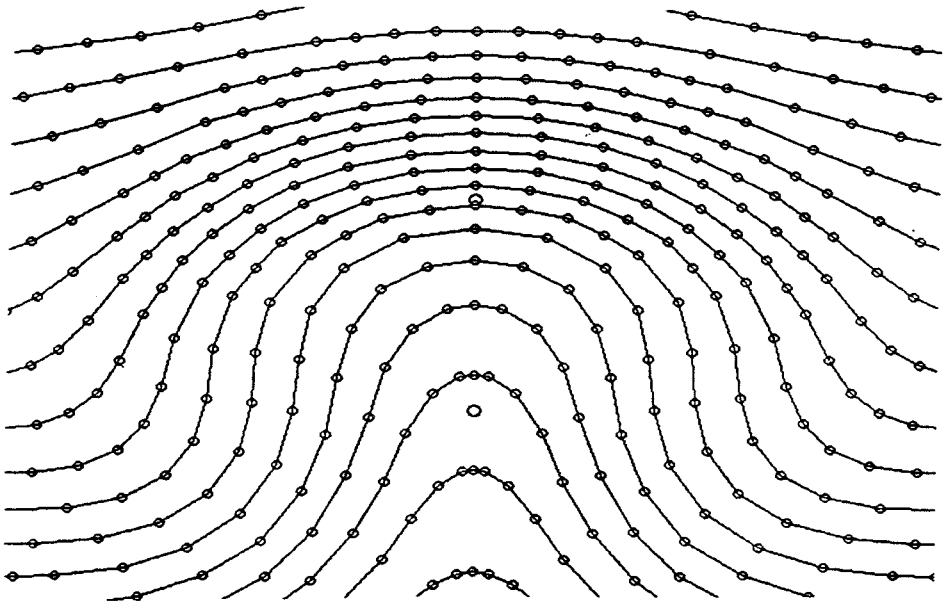

Figure 5.1. Typical total concentration field $\tilde{c}(x, z, t)$

The particles are displaced with the flow field $\vec{v}_T + \vec{v}_c$. We have:

$$\frac{d}{dt}(x_{ij}(t), z_{ij}(t)) = \vec{v}_T(x_{ij}, z_{ij}, t) + \vec{v}_c(x_{ij}, z_{ij}, t) \tag{5.8}$$

With a discrete time step Δt we have numerically:

$$x_{ij}(t + \Delta t) \simeq x_{ij}(t) + \Delta t \cdot [v_{Tx}(x_{ij}(t), z_{ij}(t), t) + v_{cx}(x_{ij}(t), z_{ij}(t), t)] \tag{5.9}$$

$$z_{ij}(t + \Delta t) \simeq z_{ij}(t) + \Delta t \cdot [v_{Tz}(x_{ij}(t), z_{ij}(t), t) + v_{cz}(x_{ij}(t), z_{ij}(t), t)] \tag{5.10}$$

The discrete representation of $\tilde{c}$ is illustrated in figure 5.2. The remaining problem is to evaluate numerically the velocity field $\vec{v}_c$, Eq. (5.3), from this discrete representation.

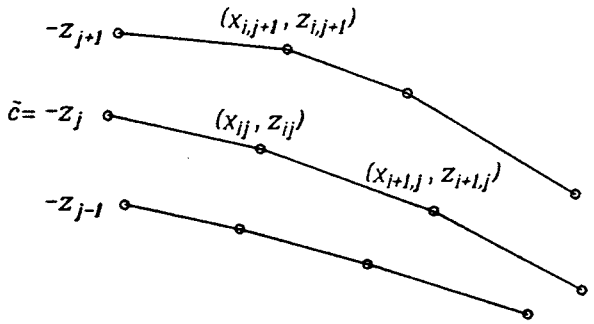

Figure 5.2. Discrete representation of $\tilde{c}$.

5.2 Evaluation of the concentration-flow integral

The analytical expression for $\vec{v}_c$ is given by the double integral (5.3). There are a number of difficulties to overcome in order to evaluate it numerically at a particular time t, knowing the particle positions (x_{ij}, z_{ij}), i.e. the approximate curves for constant $\tilde{c}$. Only a brief description of the rather intricate numerical technique is given here.

The region of integration is the whole (x', z')-plane. But c and $\partial c/\partial z'$ will be very small for large r. We choose a large region $x_- < x' < x_+$, $z_- < z' < z_+$ as the area of integration, neglecting the outside contribution.

It turns out to be better to use $\tilde{c} = -z + c$ instead of c in the integral (5.3). Then we have:

$$\vec{v}_c = -\frac{1}{2\pi}\int_{x_-}^{x_+} dx' \int_{z_-}^{z_+} dz' \frac{(x'-x, z'-z)}{(x'-x)^2+(z'-z)^2} \cdot \frac{\partial \tilde{c}(x', z', t)}{\partial z'} -$$

$$-\frac{1}{2\pi}\int_{x_-}^{x_+} dx' \int_{z_-}^{z_+} dz' \frac{(x'-x, z'-z)}{(x'-x)^2+(z'-z)^2} \cdot 1 \; - c(x, z, t)\hat{z} \tag{5.11}$$

We have for any x and z (and t) integrals of the following type:

$$I_F = \int_{x_-}^{x_+} dx' \int_{z_-}^{z_+} dz' F(x', z') \frac{\partial \tilde{c}}{\partial z'} \tag{5.12}$$

The integration in z' may be changed to an integration in $\tilde{c}$:

$$\int_{z_-}^{z_+} dz' F(x', z') \frac{\partial \tilde{c}}{\partial z'} = \left[\begin{array}{c} \tilde{c} = \tilde{c}(x', z') \\ d\tilde{c} = \frac{\partial \tilde{c}}{\partial z'} dz' \end{array} \right] = \int_{\tilde{c}_-}^{\tilde{c}_+} d\tilde{c}\, F(x', z') \tag{5.13}$$

The variable z' in $F(x', z')$ is linked to the integration variable $\tilde{c}$ by the relation $\tilde{c} = \tilde{c}(x', z')$. The integral I_F is now

$$I_F = \int_{x_-}^{x_+} dx' \int_{\tilde{c}_-}^{\tilde{c}_+} d\tilde{c}\, F(x', z') \qquad (\tilde{c} = \tilde{c}(x', z')) \tag{5.14}$$

Figure 5.3 shows the particles (i,j) in the (x',z')-plane, where $\tilde{c}_{ij} = -z_j$, and in the $(x',\tilde{c})$-plane. All particles with the same j-value lie along the straight line $\tilde{c} = -z_j$. The distance $x_{i+1,j} - x_{ij}$ between particles on the same line varies freely with i and j. The particles at the four outer borders are virtually not displaced from their initial positions.

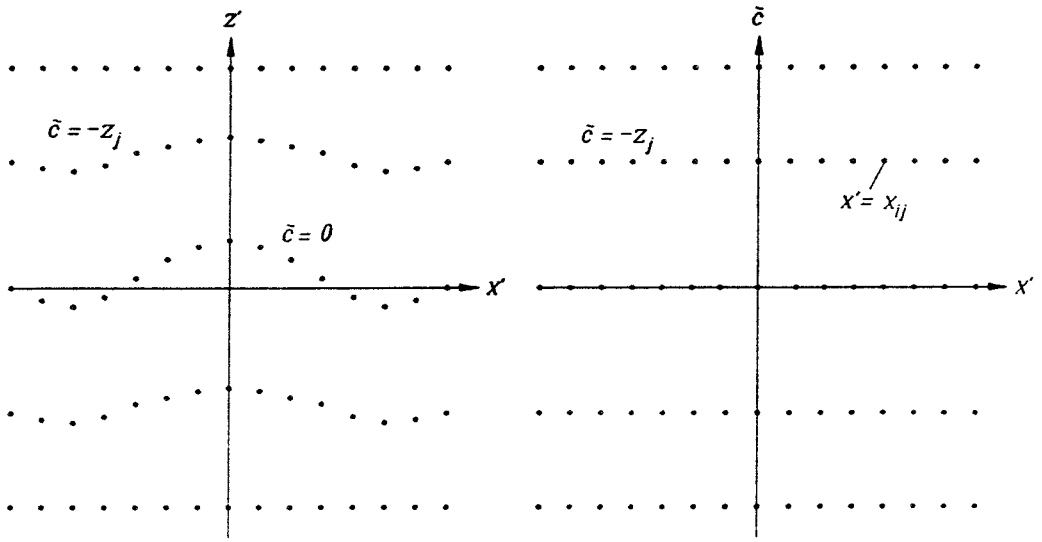

Figure 5.3. Moving particles in the (x',z')-plane and in the $(x',\tilde{c})$-plane.

The double integral I_F, Eq. (5.14), is evaluated numerically in the $(x',\tilde{c})$-plane using simple Riemann sums:

$$I_F \simeq \sum_i \sum_j \Delta x_{ij} \Delta \tilde{c}_{ij} F(x'_{ij}, z'_{ij}) \tag{5.15}$$

As increments in x we take:

$$\Delta x_{ij} = x_{i+1,j} - x_{i,j} \tag{5.16}$$

The function $F(x',z')$ is to be evaluated in the region between (x_{ij}, z_{ij}) and $(x_{i+1,j}, z_{i+1,j})$. We use the midpoint value:

$$x'_{ij} = \frac{1}{2}(x_{ij} + x_{i+1,j}) \tag{5.17}$$

$$z'_{ij} = \frac{1}{2}(z_{ij} + z_{i+1,j}) \tag{5.18}$$

For the increment $\Delta\tilde{c}_{ij}$ we use (except for the upper and lower boundary) an average from above and below:

$$\Delta\tilde{c}_{ij} = \frac{(\tilde{c}_{j+1} - \tilde{c}_j) + (\tilde{c}_j - \tilde{c}_{j-1})}{2} = \frac{\tilde{c}_{j+1} - \tilde{c}_{j-1}}{2} = \frac{-z_{j+1} + z_{j-1}}{2} \tag{5.19}$$

This gives the following Riemann sum for the double integral:

$$I_F \simeq \sum_j \frac{\tilde{c}_{j+1} - \tilde{c}_{j-1}}{2} \cdot \sum_i (x_{i+1,j} - x_{i,j}) \cdot F\left(\frac{x_{ij} + x_{i+1,j}}{2}, \frac{z_{ij} + z_{i+1,j}}{2}\right) \qquad (5.20)$$

The second double integral of (5.11) may be evaluated analytically. But we have found that it is better to evaluate it numerically. It is independent of time t, and we evaluate it for the original positions according to Eq.(5.5). Then we subtract two numerical Riemann sums, which are identical at $t = 0$. The numerical errors in the discrete formulation become significantly smaller.

We now have the following formula for $\vec{v}_c$:

$$\begin{aligned}\vec{v}_c(x,z,t) = &-\frac{1}{2\pi}\sum_j \frac{-z_{j+1} + z_{j-1}}{2} \cdot \sum_i \frac{x_{i+1,j} - x_{i,j}}{(x'_{ij} - x)^2 + (z'_{ij} - z)^2}\left(x'_{ij} - x, z'_{ij} - z\right) \\ &-\frac{1}{2\pi}\sum_j \frac{z_{j+1} - z_{j-1}}{2} \cdot \sum_i \frac{x_{i+1} - x_i}{(x'_i - x)^2 + (z'_j - z)^2}\left(x'_i - x, z'_j - z\right) \\ &-c(x,z,t)\hat{z} \qquad (5.21)\end{aligned}$$

The intermediate points $\left(x'_{ij}, z'_{ij}\right)$ are given by (5.17-18). In the second double sum, the original positions are used, and the intermediate points become:

$$x'_i = \frac{x_i + x_{i+1}}{2} \qquad z'_j = z_j \qquad (5.22)$$

5.3 Iterative solution

The positions (x_{ij}, z_{ij}) are calculated for time-step after time-step, $t = n \cdot \Delta t$. The proper choice of time-step Δt is discussed in Section 6.3.3. At the start $n = 0$, the positions are given by (5.5).

The displacement of the point i, j to the next time-step is given by Eqs. (5.9-10). The velocity $\vec{v}_T$ at the point (x_{ij}, z_{ij}) is given by an analytical expression. The salt-concentration velocity $\vec{v}_c$ is determined by formula (5.21) with $x = x_{ij}(t)$ and $z = z_{ij}(t)$. In order to get the velocity we add contributions from all points. At each time-step we have to evaluate the double sum for each point i, j.

The second double sum in (5.21) is independent of time, but the positions (x, z) change. We have evaluated the velocities for the initial positions at $t = 0$. These velocities are stored, and the velocity at any other position is obtained by linear interpolation using the four surrounding stored values.

Chapter 6

Point-source temperature field

We have seen in Section 3.6 that the characteristic time-scale t_c for salt-induced flow is much smaller than the time-scale t_T for the significant changes of the temperature field. It is therefore reasonable to consider fixed or 'frozen' temperature fields. The temperature $T(x, 0, z, t_o)$ at any fixed time t_o is used.

The instantaneous point source with a release of the heat E_o (J) at $t = 0$ at the point $(0, y_o, 0)$ is a basic case, since any other temperature field may be obtained from this one by superposition. We will in this first study only use the temperature solution for the instantaneous point source. The distance y_o must exceed the limit (4.19): $y_o > \sqrt{4at_d}$.

6.1 Temperature field

The chosen, now time-independent, temperature field in the plane $y = 0$, $T(x, z)$, is given by the point-source solution at a time t_o. We have from Eq. (4.15):

$$T(x, z) = T(r) = \frac{E_o}{C(4\pi a t_o)^{3/2}} e^{-y_o^2/(4at_o)} \cdot e^{-r^2/(4at_o)} + T_o(z) \tag{6.1}$$

Here, $r = \sqrt{x^2 + z^2}$ is the radial distance in the flow plane $y = 0$.

The corresponding dimensionless excess temperature T' is in accordance with (2.8):

$$T' = \frac{T - T_o(z)}{T_1} = A_o \cdot e^{-(r')^2 L_1^2/(4at_o)} \tag{6.2}$$

As scale length we choose:

$$L_1 = \sqrt{4at_o} \tag{6.3}$$

The dimensionless excess temperature T' is then

$$T'(r') = A_o e^{-(r')^2} \tag{6.4}$$

The *dimensionless temperature amplitude* A_o is from (6.1-2), inserting (2.43) for T_1:

$$A_o = \frac{\alpha_T E_o}{\pi\sqrt{\pi}\alpha_c c_z^o C} \cdot \frac{1}{(4at_o)^2} e^{-y_o^2/(4at_o)} \qquad (y_o > \sqrt{4at_d}) \tag{6.5}$$

The use of the instantaneous point source requires that the restriction (4.19) is fulfilled.

6.2 Numerical model

The numerical model described in Chapter 5 is used with the particular temperature field T' from the point source at a time t_o. Let us summarize the complete set of equations used.

The problem is solved in the dimensionless formulation. The temperature field and the ensuing dimensionless velocity component $\vec{v}_T$ are from (3.37) and (3.34-36) with $\rho = -T'$, $\rho_1 = A_o$ and $r_1 = 1$:

$$T' = A_o \cdot e^{-(r')^2} \tag{6.6}$$

$$v_{Tx} = \frac{A_o}{2} \cdot \frac{2x'z'}{((x')^2 + (z')^2)^2} \left[1 - (1 + (r')^2)e^{-(r')^2}\right] \tag{6.7}$$

$$v_{Tz} = \frac{A_o}{2} \cdot \left\{ \frac{(z')^2 - (x')^2}{((x')^2 + (z')^2)^2} \left[1 - (1 + (r')^2)e^{-(r')^2}\right] + e^{-(r')^2} \right\} \tag{6.8}$$

The dimensionless amplitude factor A_o is given by (6.5), and the scale length L_1 by (6.3).

The dimensionless velocity component $\vec{v}_c$ from the salt-induced flow is according to Section 3.3 determined by the equations:

$$\nabla^2 P_c + \frac{\partial c'}{\partial z'} = 0 \qquad \vec{v}_c = -\nabla' P_c - c'\hat{z} \tag{6.9}$$

This leads to the integral (5.3), which is used in the numerical model to determine $\vec{v}_c$.

Finally, the total dimensionless salt concentration $\tilde{c} = -z' + c'$ is displaced by the velocity $\vec{v}_T + \vec{v}_c$ as described mathematically by the salt balance equation (5.1):

$$\frac{\partial \tilde{c}}{\partial t'} + \nabla' \cdot [\tilde{c}(\vec{v}_T + \vec{v}_c)] = 0 \tag{6.10}$$

It is noteworthy that the above dimensionless problem contains only *one parameter*, namely the dimensionless temperature amplitude A_o.

6.3 Numerical results

The coupled process has been calculated with the numerical model for values on A_o from 0.3 to 100. In the case $A_o = 3$, we have made more detailed studies of mesh choice.

6.3.1 Temperature flow component $\vec{v}_T$

The dimensionless flow has the two components $\vec{v}_T$ and $\vec{v}_c$. There is an option in the computer model for which the latter flow $\vec{v}_c$ is suppressed. We get the flow of the salt particles due to the temperature flow $\vec{v}_T$ only. This is not our physical situation, but it provides an insight into the complexity of our problem.

The result for $A_o = 3$ is shown in Figures 6.1A-E on page 37. The figures show the curves of constant dimensionless total concentration $\tilde{c}$ for $t' = 1, 2, 4, 8$ and 10, respectively. The $\tilde{c}$-curves at the beginning $t' = 0$ are horizontal, straight lines. The water moves upwards in the central warm region. Further out it follows the dipole field shown in Figure 3.1.

There are stagnation points for $\vec{v}_T$ at $(\pm 1.12, 0)$. There is a vortex motion around the two stagnation points, which complicates the behaviour around them. The $\tilde{c}$-curves are dragged into the vortex, and they spiral between each other.

The salt-flow component $\vec{v}_c$ will moderate the flow process. We will see below how the upward flow in the warm region is counteracted and eventually balanced by the weight of heavier water coming from below.

6.3.2 The case $A_o = 3$

As the first case we take $A_o = 3$, which represents a moderate heating and flow process. A coarse, an intermediate and a fine initial mesh are compared. About the same number of points are used in the three cases. The mesh gives the starting positions (x_i, z_j) of the particles. The intermediate mesh consists of $33 \cdot 21$ points. It is shown in Figure 6.2A on page 38. The figure shows a central, rectangular region $-4 < x' < 4, -2 < z' < 5$. The vertical and horizontal spacing is here 0.5. The two thicker circles show here and in the following figures the center position $(0, 0)$ and the point $(0, 1)$. The computational points cover the larger rectangle $-8 < x' < 8, -4 < z' < 6$.

Figures 6.2B-J show the $\tilde{c}$-curves for $t' = 1, 2, ...9$. We see that the model represents the spiral motion around the vortex quite well. At $t' = 6$, there is a very sharp point in the vortex for the curve $\tilde{c} = 0.5$. At $t' = 7.5$, there is an error as the curve crosses itself near the sharp point. This error continues and increases somewhat at $t' = 8$ and $t' = 9$. But the method is quite stable, and the error in the complicated vortex motion does not significantly disturb the solution outside the vortex.

The result for the coarse initial mesh is given in Figure 6.3A-D on pages 39-40. The initial spacing vertically and horizontally is 1. The number of points are $31 \cdot 20$, so the computational region is now much larger: $-15 < x' < 15, -10 < z' < 10$. The figures show here as in all other cases a smaller central region. The result is pretty much the same as for the intermediate mesh except for the central vortex part, where the finer details are lost. We can conclude from this comparison of the coarse and intermediate meshes that it is sufficient to use the smaller computational area of the intermediate mesh.

The central part of the fine initial mesh is shown in Figure 6.4A on page 40. The fine spacing is only 0.2 units in the horizontal and vertical directions. The computational region is limited to the rectangle $-4 < x' < 4, -2 < z' < 4$, since we here focus on the vortex behaviour. The calculations are less stable, since the particles are so close to each

other. At $t' = 3$, there is some rippling for the curve $\tilde{c} = -0.6$. This is increased at $t' = 4$. The calculations with finer mesh are less stable.

From these comparisons we conclude that the best result is obtained with the intermediate mesh.

6.3.3 Numerical problems and remedies

We have had a number of problems with the numerical model and its application in particular for large A_o.

One problem has been that the particles may *accumulate* in a small area. This can be seen in Figure 6.1C-D that shows the $\vec{v}_T$-field only. The particles from below move towards the z'-axis and accumulate near the axis. They move upwards very close to the z'-axis. This leads to numerical problems, since we divide by the distance from a particle to the midpoint between consecutive particles in Eq.(5.21). A particle is therefore *removed*, when the distance between any two particles on the same $\tilde{c}$-curve fall below a value Δs_{min}. This value is an input to the program. In the calculation we normally take $\Delta s_{min} = \Delta x_{min}/5$.

Another problem is that the particles *separate* from each other so that certain areas become virtually empty. This may also be seen in Figure 6.1C-D. Above the center (0,0) near the z'-axis the particles move away from the axis. New particles are therefore *inserted*, when the distance between two particles on the same $\tilde{c}$-curve exceeds a value Δs_{max}. This value is an input to the model. We do this in the central region, where the initial horizontal distance is Δx. A normal choice has been $\Delta s_{max} = 1.5 \cdot \Delta x$.

A third problem is that two $\tilde{c}$-curves may come very close to each other. The problem occurs when a particle lie very close to a midpoint of an adjacent $\tilde{c}$-curve. The particle is removed if the distance falls below an input value $\Delta s'_{min}$. This limit must be quite small, since the $\tilde{c}$-curves lie very close above the warm region. We choose $\Delta s'_{min} = \Delta z_{min}/50$.

Particles are flowing upwards into the warm region. The particles at the lower parts of the vertical boundary will eventually be moved inwards. This occurs for calculations during a long time, i.e. for large t'. A new particle is inserted at the boundary on the initial level if the distance from the boundary particle to the initial boundary position exceeds Δx.

This removal and insertion of particles require a renumbering in the program so that the particles (x_{ij}, z_{ij}) on a $\tilde{c}$-curve lie in the right order. We shall move along the $\tilde{c}$-curve from the left boundary to the right one, when i is increased step by step.

The $\tilde{c}$-curves are indicated in Figure 5.3, left. To the right we have a representation in the $(x', \tilde{c})$-plane. A particular complication in this representation is the case, when the $\tilde{c}$-curves become strongly curved as in Figures 6.2E-J. For given values of $\tilde{c}$ and x', we may have three points at different z'-values. This will mean that the points along a $\tilde{c}$-line in Figure 5.3, right, moves up to a certain x'-value, then there are consecutive points with decreasing x'-values, and after that the points lie again in a row with increasing x'-values for increasing i. The model works quite well also in this case. Then some of the increments Δx_{ij} in (5.15) are negative, and their contribution to the Riemann sum changes sign. This is consistent with the fact that the derivative $\partial\tilde{c}/\partial z'$ in (5.12) is positive in these points, while it normally is negative, since $\tilde{c}$ increases downwards.

The technique described in Section 5.2, where the calculations are performed in the

$(x', \tilde{c})$-plane, is a very particular one. I think that a main advantage compared to conventional numerical techniques is that it can cope so easily with these complicated, intertwined vortex curves.

The problem to represent the vortex curves increases with time. This is illustrated in Figures 6.2F-J and 6.9C-F (page 45). We need more and more particles to represent the intertwined curves. But, physically, these curves neutralize each other at a certain distance away. In order to obtain the best result for the vertical displacement above the warm region, one shall represent the vortex on an intermediate level.

The time-step Δt is chosen, so that the largest displacement $(= (A_o/2) \cdot \Delta t)$ at the start is given. This displacement is an input in the model. Normally we choose this length to $\Delta z_{min}/5$.

The velocity $\vec{v}_T$ and our problem is symmetrical relative to the z'-axis. The velocity integral (5.21) giving $\vec{v}_c$ need only to be calculated for particles lying in $x' \geq 0$, but the sum over i and j must of course be performed for all particles.

6.3.4 Results for different A_o

Figures 6.5-9 on pages 41-45 show the result for $A_o = 0.3, 1, 10, 30$ and 100. About $30 \cdot 20 = 600$ initial particles are used in all cases. The process is quite different for small and large A_o, since the thermal velocity $\vec{v}_T$ is directly proportional to A_o. The choice of mesh must be adapted accordingly. With a judicious choice we feel that is has been sufficient to start with the 600 particles. The computer time on an IBM-486 personal computer became 10 to 30 minutes, with the longer time for higher A_o.

The result for $A_o = 0.3$, shown in Figure 6.5A-D, is not dramatic. The same behaviour, shown in Figure 6.6A-H, is obtained for $A_o = 1$. The vortex motion is suppressed by the salt density term $-c'\hat{z}$. The vortex occurs for $A_o = 3$ and becomes increasingly stronger for increased A_o. It is easier to extend the calculations to larger times t' for small A_o, for which the process is less dramatic. We have for $A_o = 1$, Figure 6.6, continued the calculations to $t' = 18$. The curves for $t' = 10, 15$ and 18 are almost identical. There is a small residual horizontal movement upwards and outwards around the level $z' = 0.8$ and an inward movement around the level $z' = -0.5$.

The results for $A_o = 3$ was shown in Figure 6.2. The case $A_o = 10$ is shown in Figure 6.7A-F. The vortex motion is quite strong, and after $t' = 2$ we have trouble to represent it properly. The spiral curves begin cross each other at $t' = 2.5$. We have continued the calculations until $t' = 6.5$. The curves in the vortex become more and more entangled. The model can, perhaps somewhat suprisingly, still produce stable results outside the vortex region.

The results for $A_o = 30$ and 100 are shown in Figure 6.8A-C and 6.9A-F, respectively. The process is now much more intense. Water is rapidly moved upwards to a quasi steady-state position. The case $A_o = 100$ is shown for several times to illustrate the complicated vortex motion. The spirals start to cross each other at $t' = 0.5$, Figure 6.9C. The complications increase for $t' = 1, 2$ and 6 according to the following figures 6.6D-F. The different intertwined $\tilde{c}$-curves neutralize each other. The salt will be mixed in the vortex region, and the precise positions do not really matter. Therefore, we feel that the result outside the vortex is still valid with an acceptable accuracy.

6.3.5 Largest upward displacement

A main goal in this study is to estimate the upward motion in order to assess the effect of the salt barrier. We are in particular interested in the particles that start in the warm region, where the potentially leaking canisters lie. We have seen in the above results that the largest upward motion from the warm central region occurs along the symmetry line $x' = 0$, i.e. the z'-axis.

Consider a particle that starts at $(0, z_o)$ at $t' = 0$. It will move upwards along the z'-axis. The position at t' is denoted $z_m(t', z_o)$:

$$(x_p, z_p) = (0, z_m(t', z_o)) \qquad z_m(0, z_o) = z_o \tag{6.11}$$

We use a special notation for the largest value for large t':

$$z'_{max}(z_o) = z_m(\infty, z_o) \tag{6.12}$$

We are in particular interested in the particle that starts from the center $z_o = 0$ closest to the canister s, i.e. in $z_m(t', 0)$ and $z'_{max}(0)$.

Figure 6.10 on page 46 shows $z_m(t', 0)$ from the calculations for $A_o = 3$ for the three meshes: intermediate (Figure 6.2), coarse (Figure 6.3) and fine (Figure 6.4). The difference between the curves is an indication of the numerical uncertainty. We believe that the intermediate mesh, i.e. the middle curve, gives the best result. The largest value $z'_{max}(0)$ is around 1.2. Figure 6.11 shows $z_m(t', z_o)$ for z_o from -2.5 to +2 for the intermediate mesh. The points above $z_o = 1.5$ and below $z_o = -2$ attain a reasonably constant value after $t' \simeq 1.5$, while there is a longer time-scale in the central region. The particle that starts at $z_o = -1.5$ has the longest time-scale. There is a *separation point* between $z_o = -2$ and $z_o = -1.5$. The particles below this point attain an equilibrium below the warm region, while particles above it are sucked into the warm region with its high velocities v_{Tz}, and they end above $z' = 0$.

The maximal upward displacements $z_m(t', z_o)$ are shown for $A_o = 0.3, 1, 10, 30$ and 100 in Figures 6.12-16 on pages 46-48. The case $A_o = 10$ is shown in greater detail in Figure 6.14. We see that $z'_{max}(0)$ is around 1.9. The point of separation lies between $z_o = -3$ and -1.5. The point of separation moves downwards with increasing A_o. It lies between $z_o = -4.5$ and -3 for $A_o = 30$, and between $z_o = -8$ and -6 for $A_o = 100$.

The maximal displacement for $z_o = 0$,1 and -1 according to the above results is given in Table 6.1. This table is a main result of the study.

A_o	0.3	1	3	10	30	100
$z'_{max}(0)$	0.24	0.7	1.2	1.9	2.7	4.1
$z'_{max}(1)$	1.1	1.3	1.6	2.1	3.0	4.4
$z'_{max}(-1)$	-0.9	-0.3	0.9	1.6	2.4	4.0

Table 6.1. Maximal displacement $z'_{max}(z_o)$ from $(0, z_o)$ for different A_o according to numerical calculations.

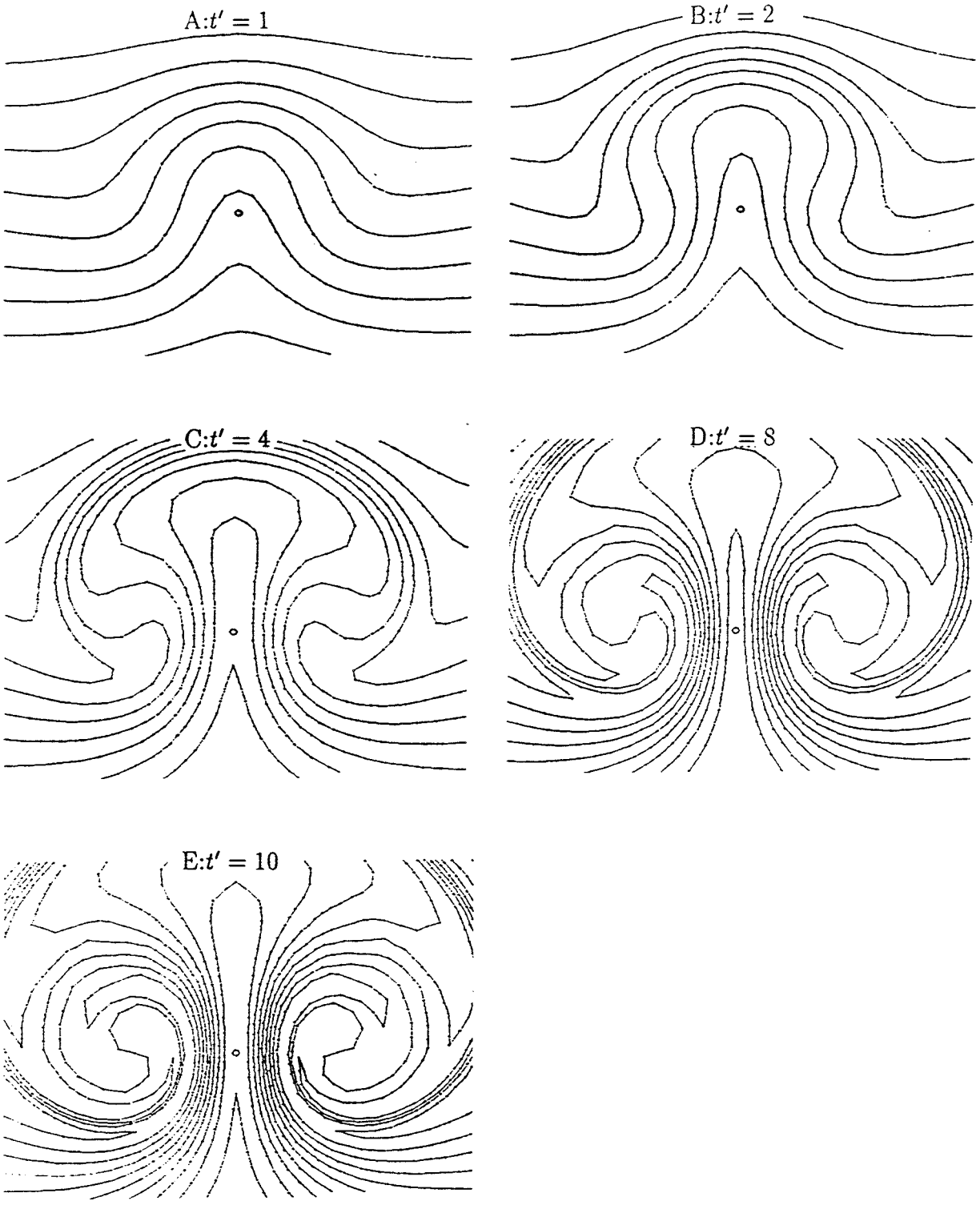

Figure 6.1. Curves of constant $\tilde{c}$ due to the temperature flow component $\vec{v}_T$ only ($\vec{v}_c = \vec{0}$), $A_o = 3$.

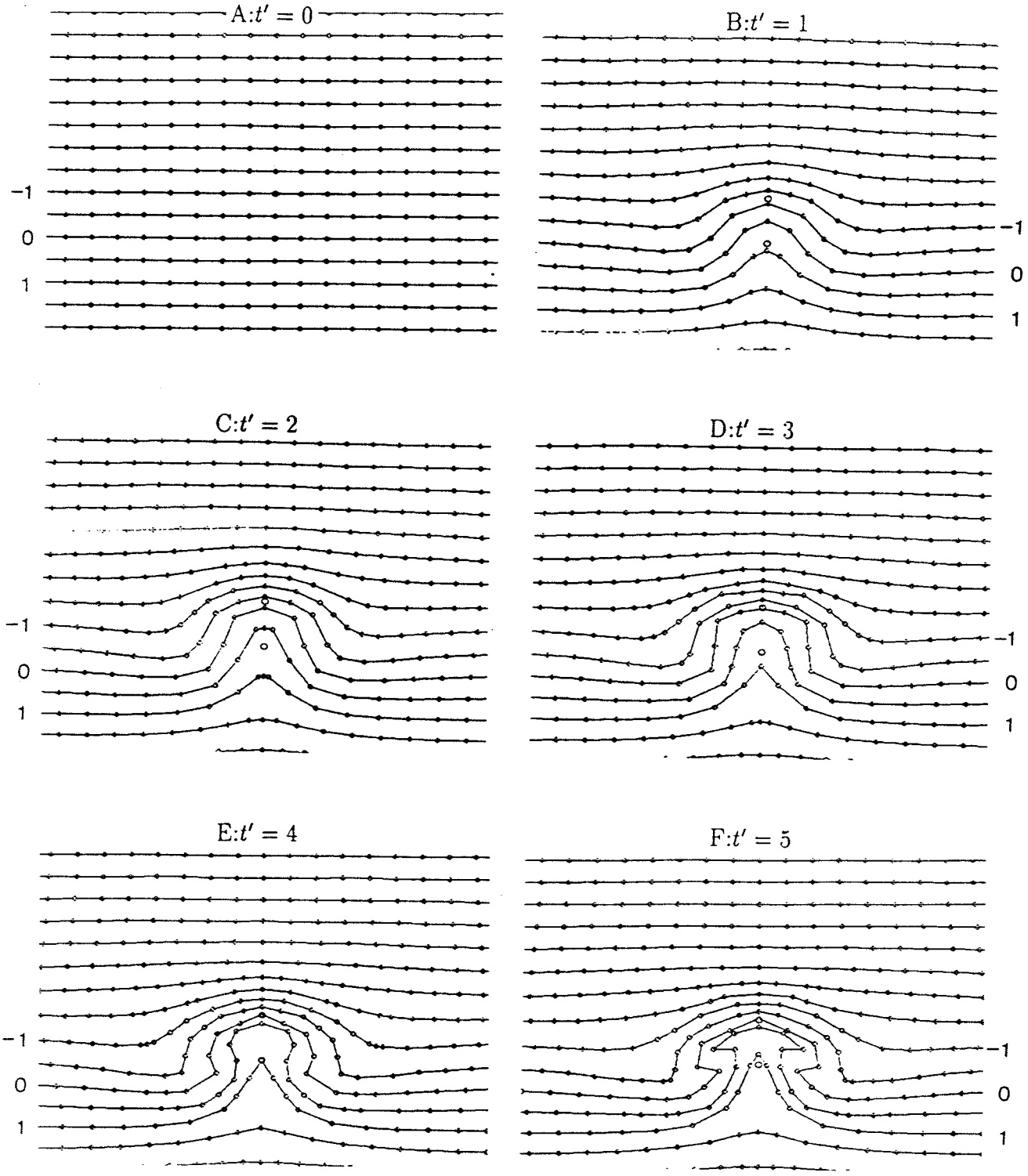

Figure 6.2. Curves of constant $\tilde{c}$ for $A_o = 3$ with the intermediate initial mesh.

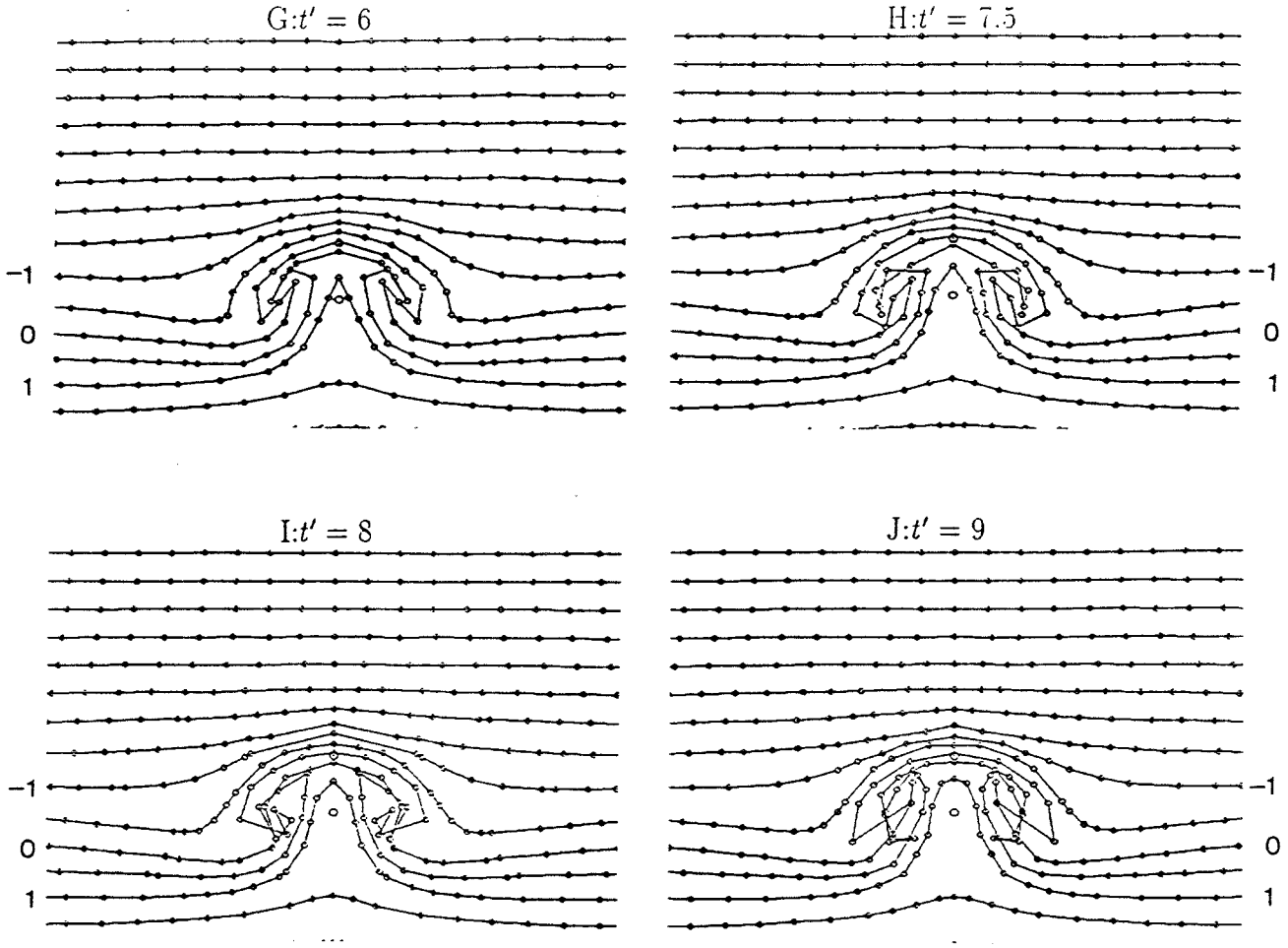

Figure 6.2. Curves of constant $\tilde{c}$ for $A_o = 3$ with the intermediate initial mesh.

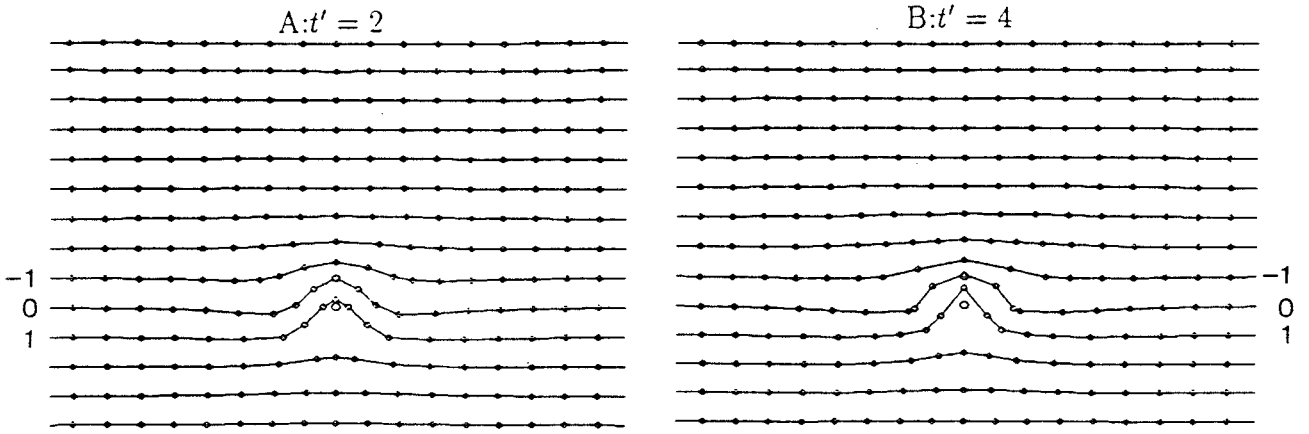

Figure 6.3. Curves of constant $\tilde{c}$ for $A_o = 3$ with the coarse initial mesh.

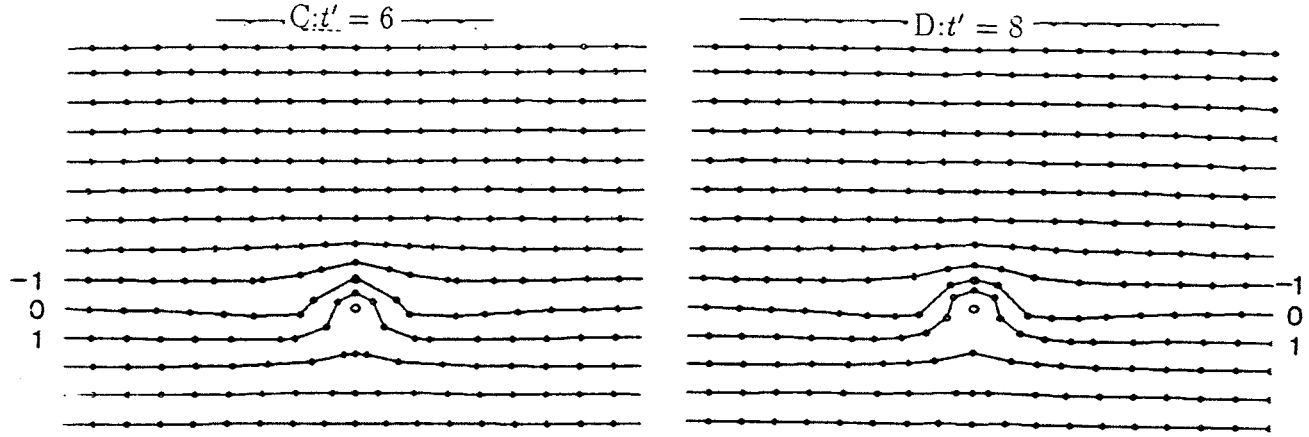

Figure 6.3. Curves of constant $\tilde{c}$ for $A_o = 3$ with the coarse initial mesh.

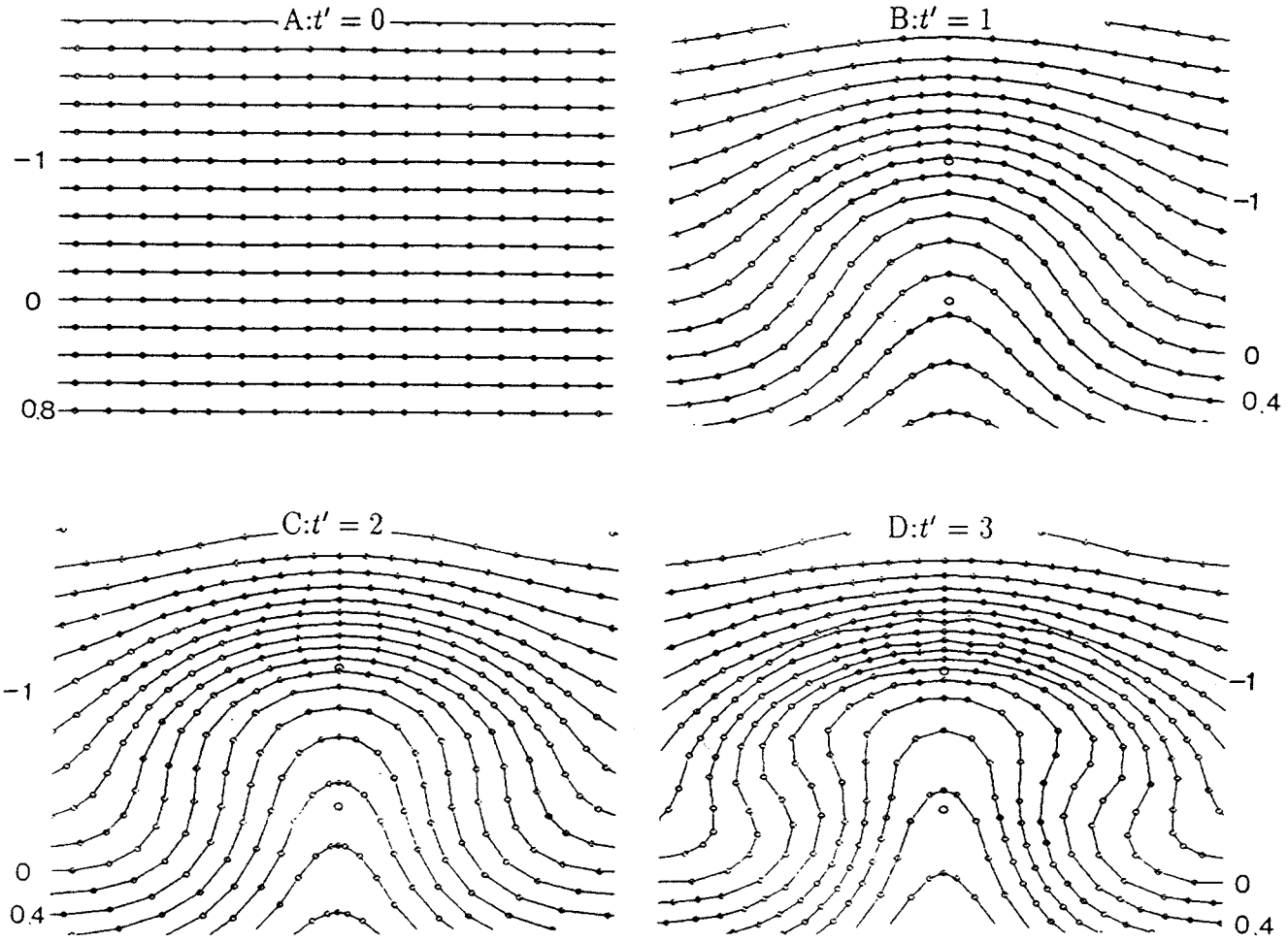

Figure 6.4. Curves of constant $\tilde{c}$ for $A_o = 3$ with the fine initial mesh.

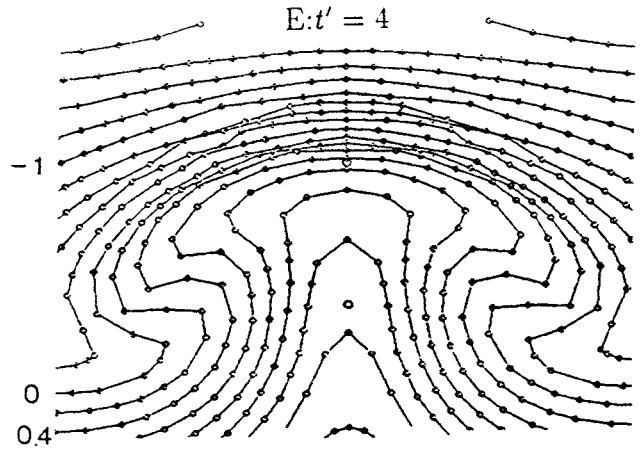

Figure 6.4. Curves of constant $\tilde{c}$ for $A_o = 3$ with the fine initial mesh.

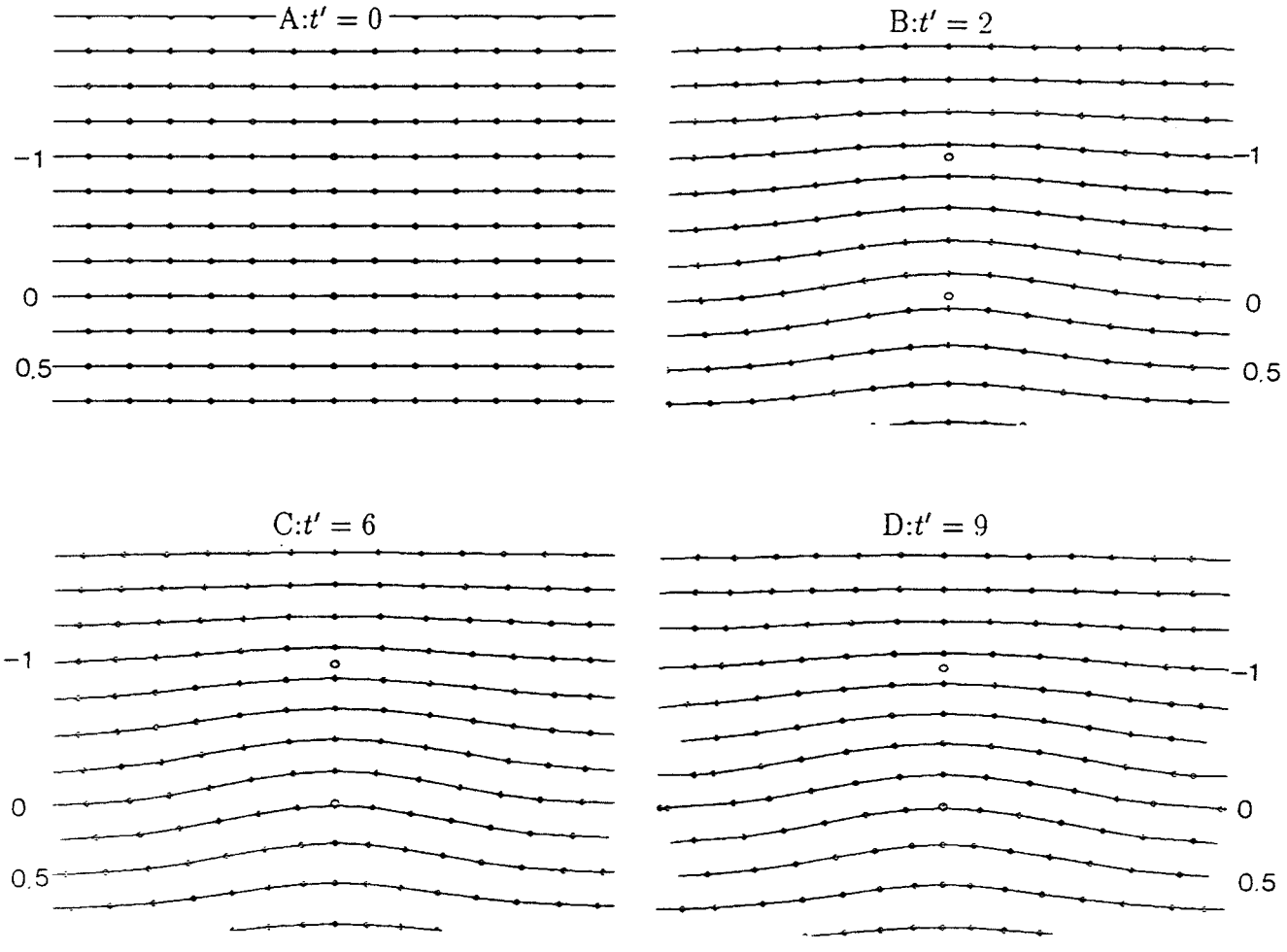

Figure 6.5. Curves of constant $\tilde{c}$ for $A_o = 0.3$.

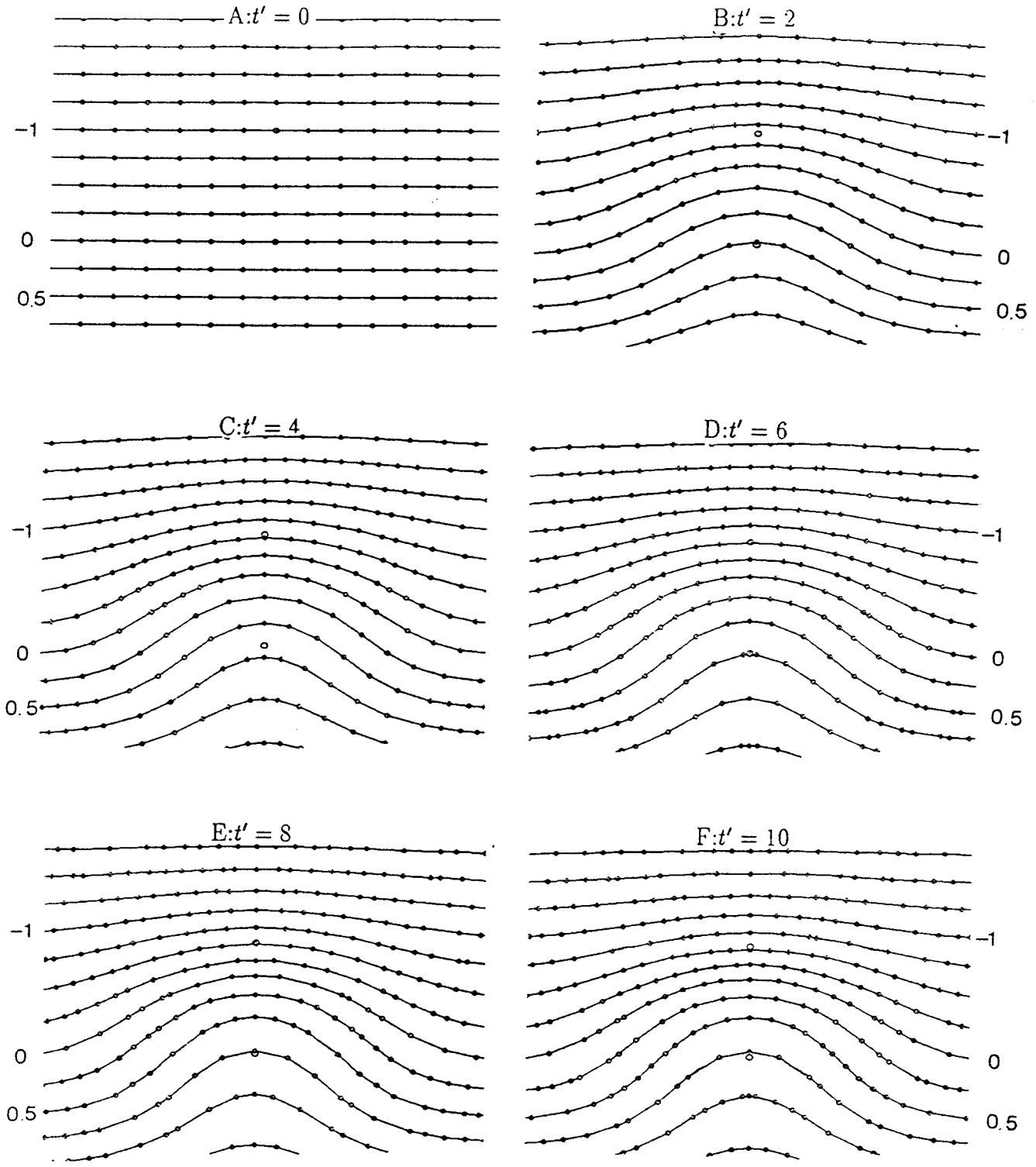

Figure 6.6. Curves of constant $\tilde{c}$ for $A_o = 1$.

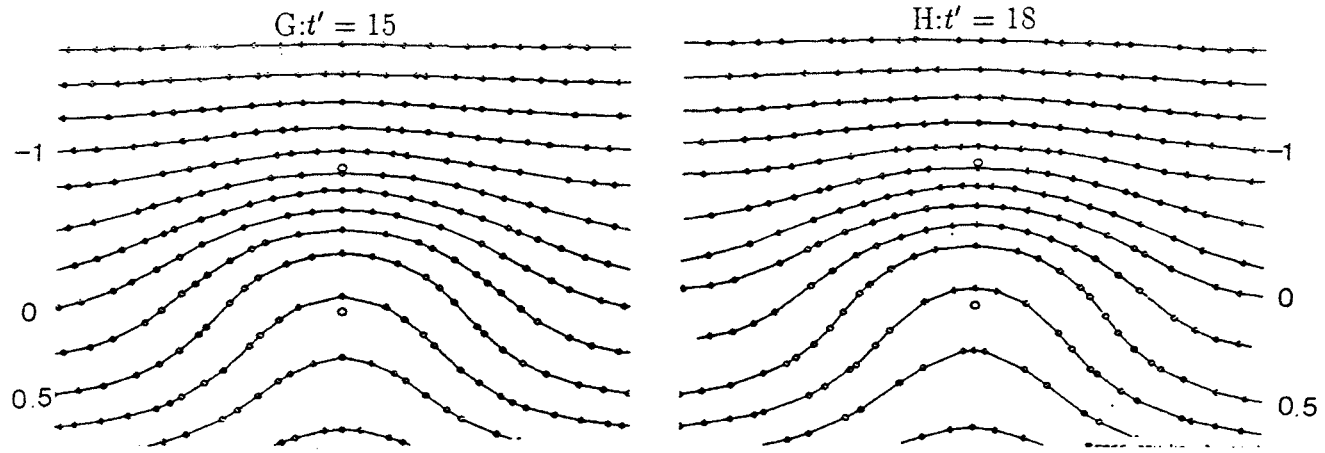

Figure 6.6. Curves of constant $\tilde{c}$ for $A_o = 1$.

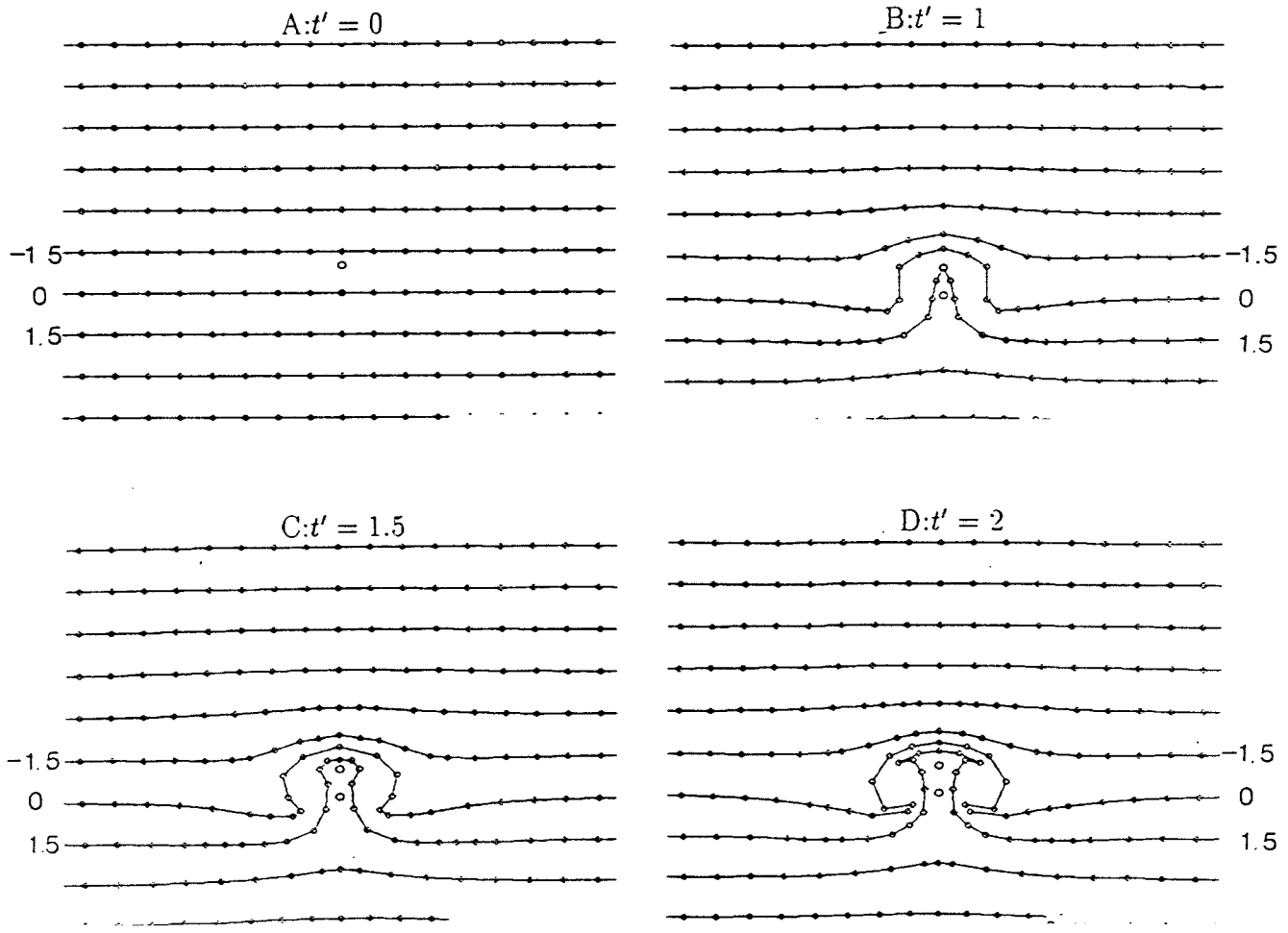

Figure 6.7. Curves of constant $\tilde{c}$ for $A_o = 10$.

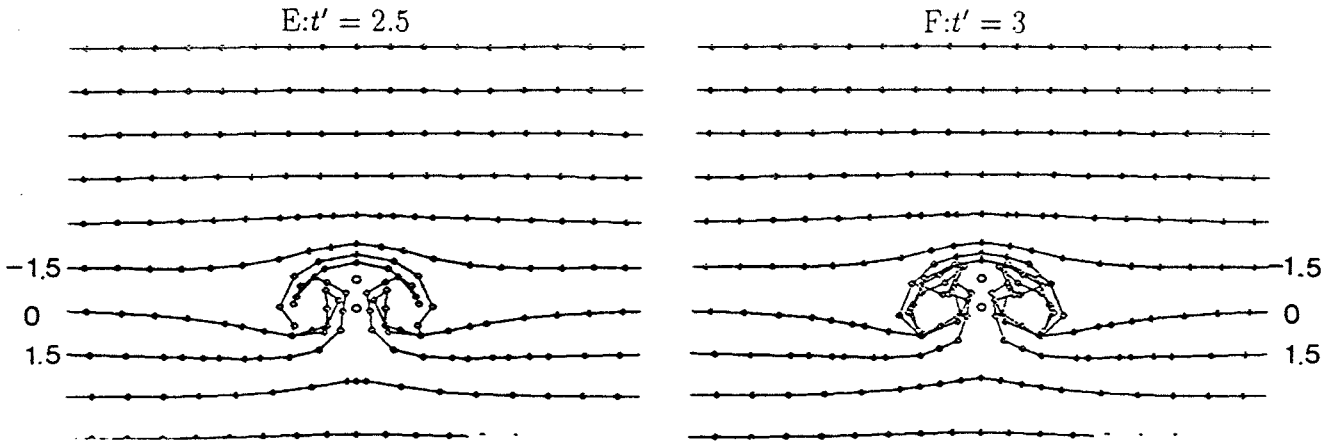

Figure 6.7. Curves of constant $\tilde{c}$ for $A_o = 10$.

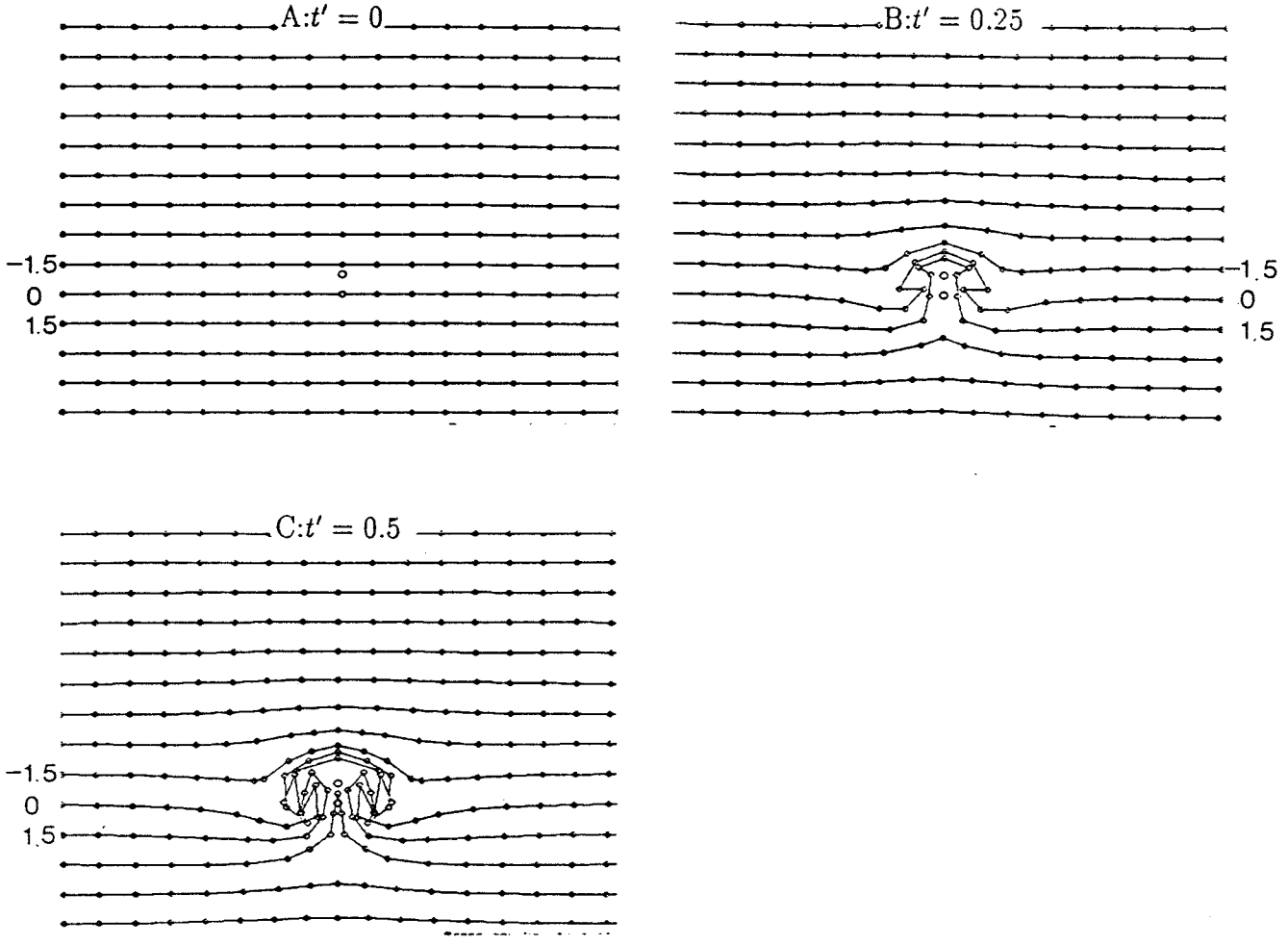

Figure 6.8. Curves of constant $\tilde{c}$ for $A_o = 30$.

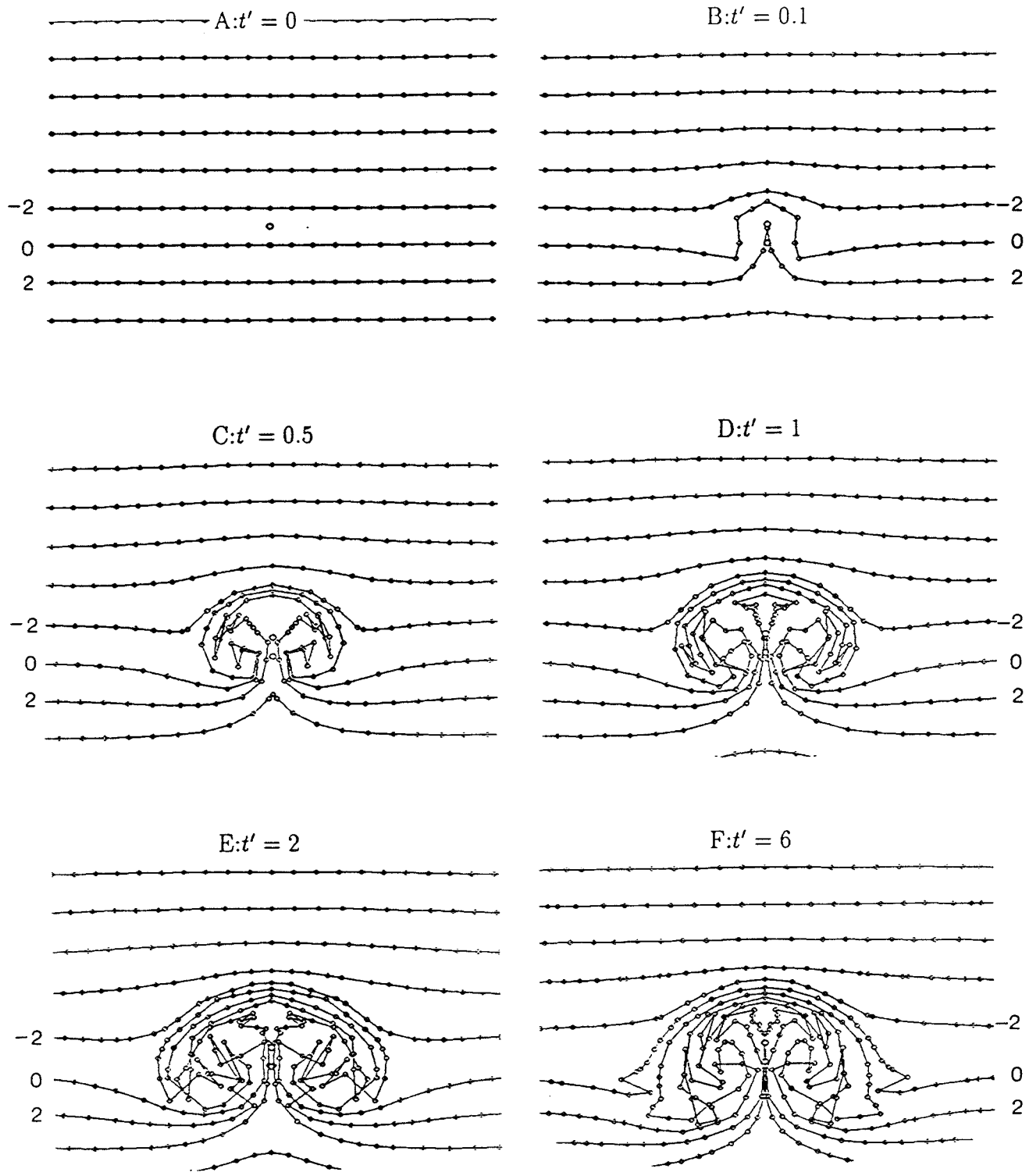

Figure 6.9. Curves of constant $\tilde{c}$ for $A_o = 100$.

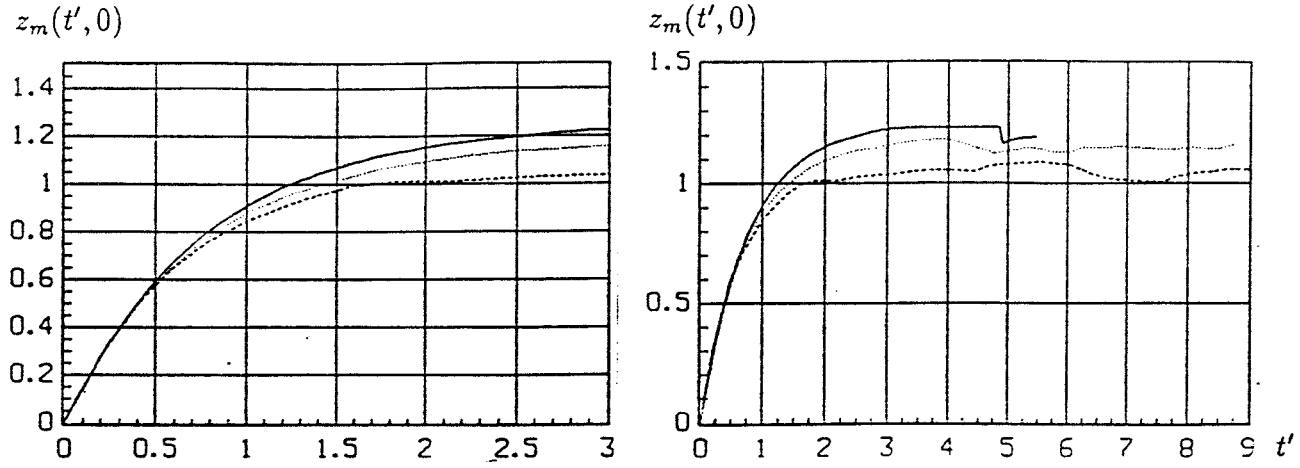

Figure 6.10. Displacement $z_m(t',0)$ along the z'-axis for $A_o = 3$ for the fine (-), intermediate (...) and coarse (- -) initial meshes.

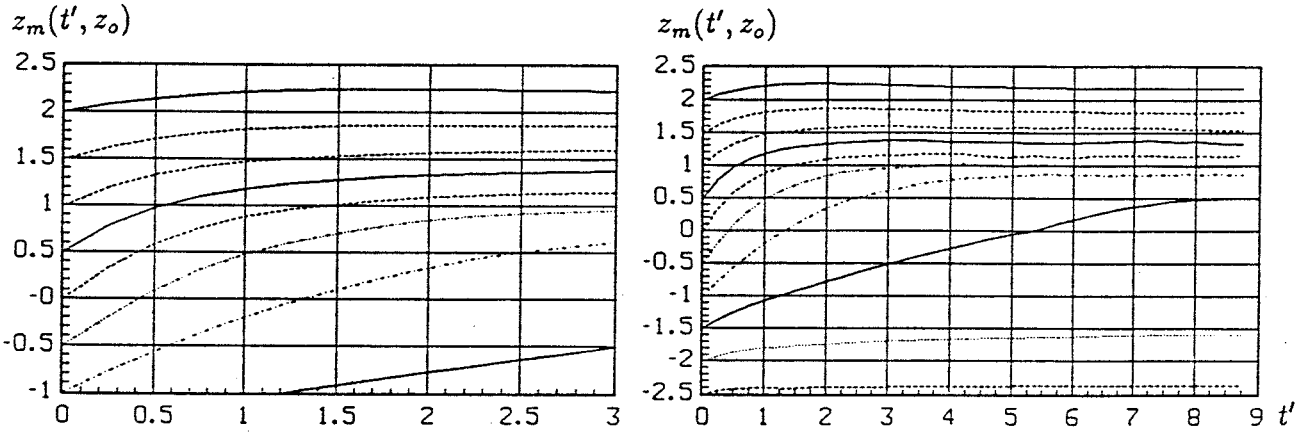

Figure 6.11. Displacement $z_m(t', z_o)$ along the z'-axis for $A_o = 3$ for different z_o.

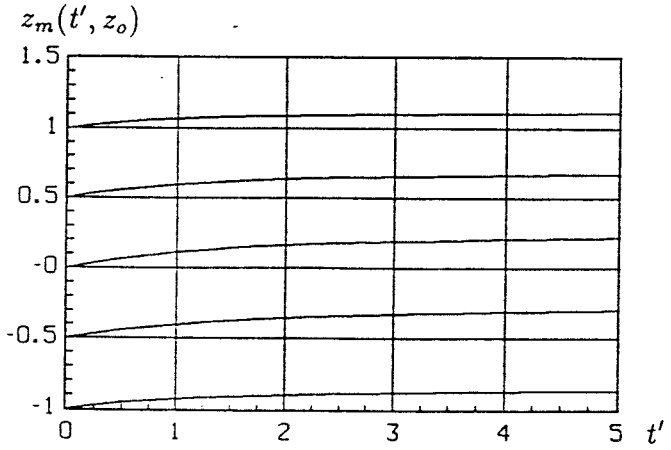

Figure 6.12. Displacement $z_m(t', z_o)$ for $A_o = 0.3$.

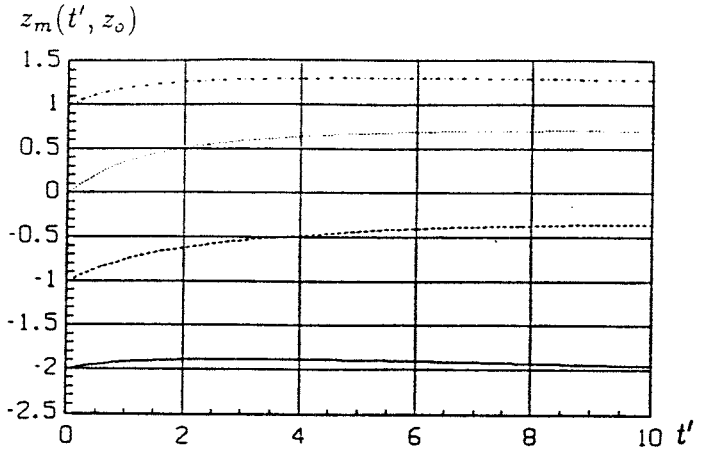

Figure 6.13. Displacement $z_m(t', z_o)$ for $A_o = 1$.

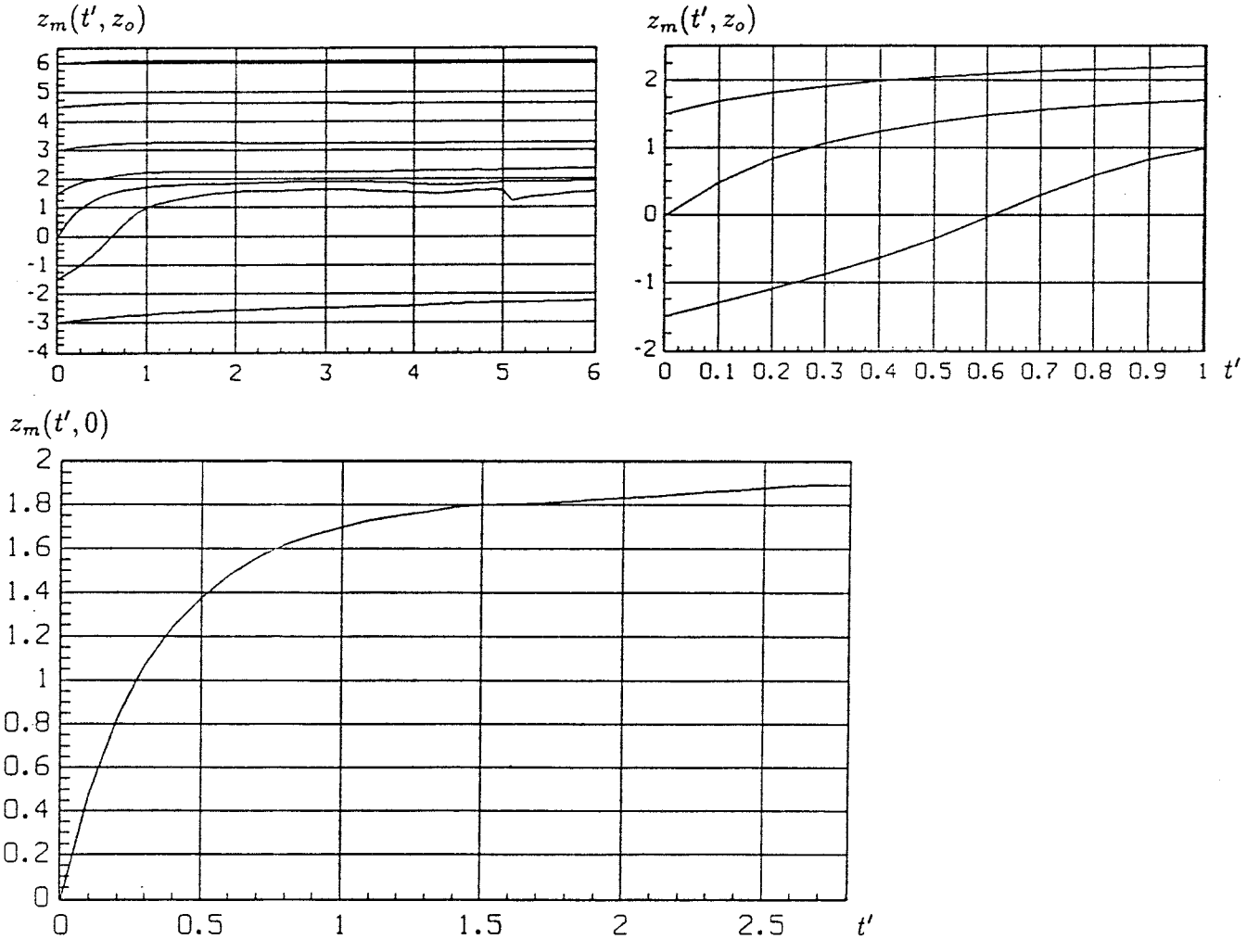

Figure 6.14. Displacement $z_m(t', z_o)$ for $A_o = 10$.

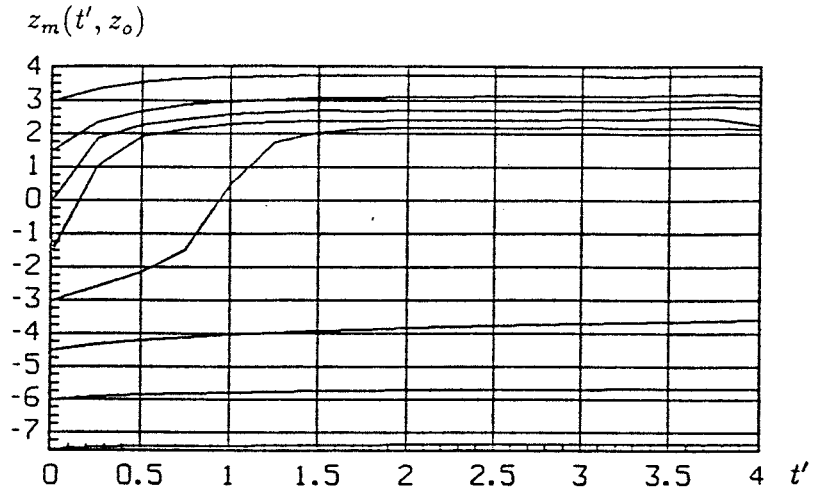

Figure 6.15. Displacement $z_m(t', z_o)$ for $A_o = 30$.

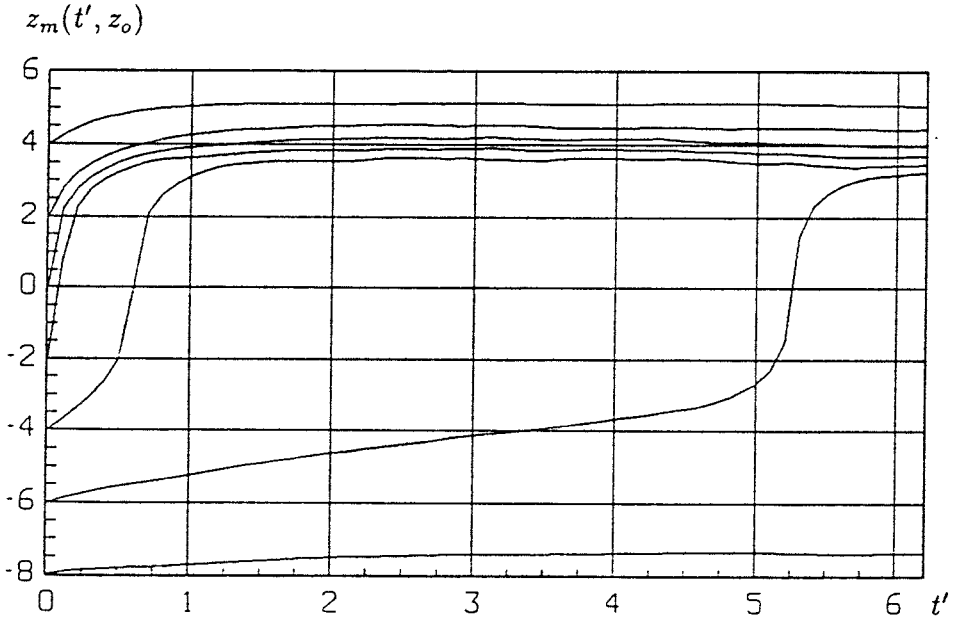

Figure 6.16. Displacement $z_m(t', z_o)$ for $A_o = 100$.

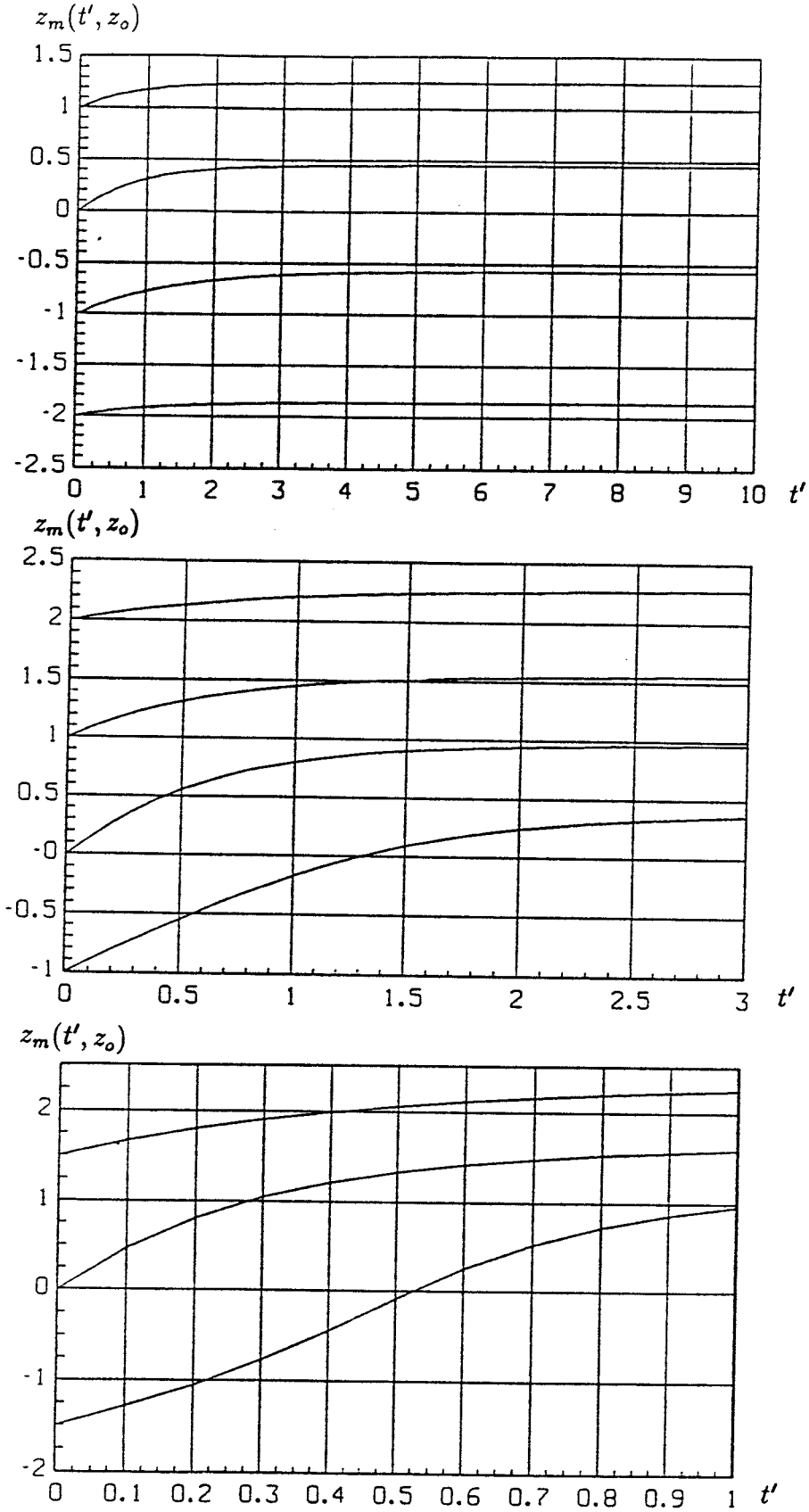

Figure 6.17. Displacement $z_m(t', z_o)$ for $A_o = 1$ (top) ,3 (middle) and 10 (bottom) from the integral (6.19).

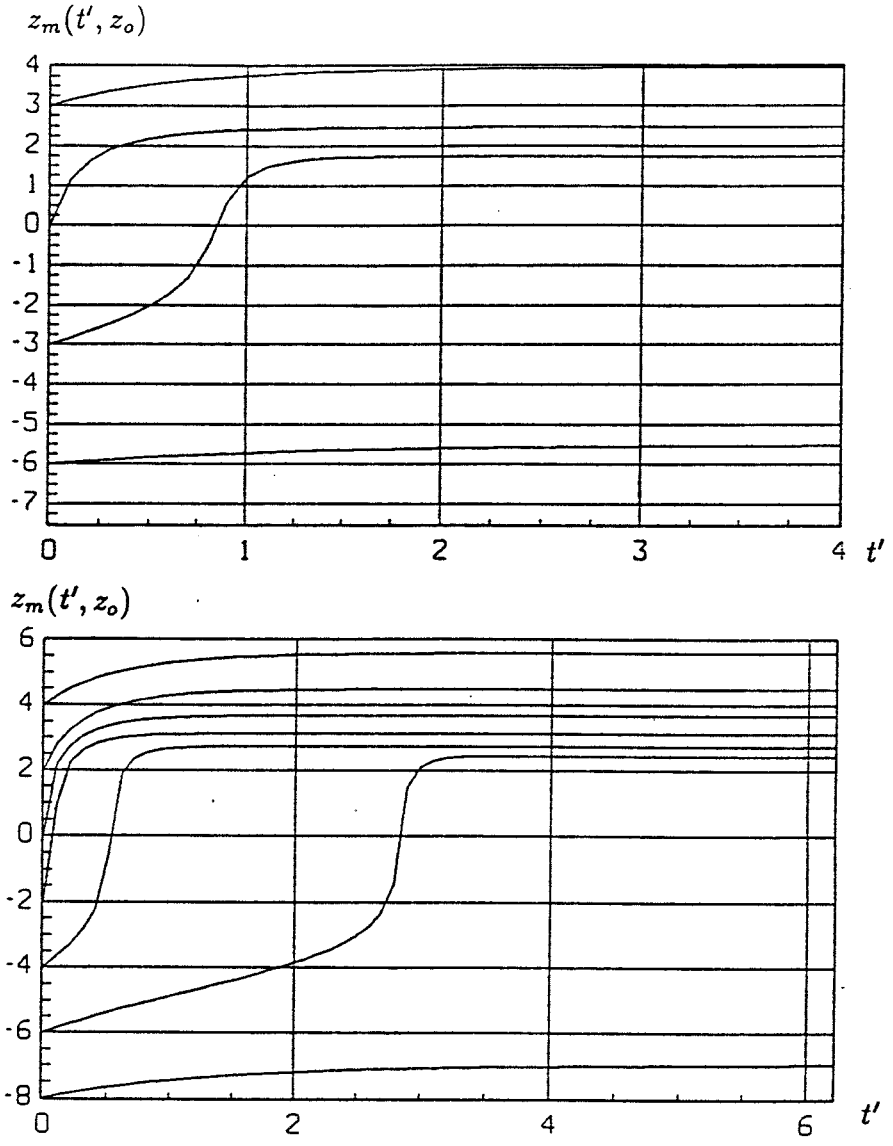

Figure 6.17. Displacement $z_m(t', z_o)$ for $A_o = 30$ (top) and 100 (bottom) from the integral (6.19).

6.4 Upward flow along the z'-axis

The largest upward displacement, which occurs along the z'-axis above the warm region, may be obtained analytically, if the contribution from the salt concentration field P_c is *neglected.* We use the approximation:

$$\vec{v}_T + \vec{v}_c = \vec{v}_T - \nabla' P_c - c'\hat{z} \simeq \vec{v}_T - c'\hat{z} \tag{6.13}$$

In this approximation, the equations for a salt particle $(x_p(t'), z_p(t'))$ become:

$$\frac{dx_p}{dt'} = v_{Tx}(x_p, z_p) \tag{6.14}$$

$$\frac{dz_p}{dt'} = v_{Tz}(x_p, z_p) - (z_p(t') - z_p(0)) \tag{6.15}$$

The temperature flow field $\vec{v}_T$ is given by (6.7-8).

6.4.1 Equation for $z_m(t', z_o)$

On the z'-axis, we have $x_p(t') = 0$ and $v_{Tx} = 0$. For $z_p(t') = z_m(t', z_o)$ we have:

$$\frac{dz_m}{dt'} = v_{Tz}(0, z_m) - z_m + z_o \tag{6.16}$$

Eq.(6.8) with $x' = 0$ and $z' = z_m$ gives:

$$\frac{dz_m}{dt'} = \frac{A_o}{2} \cdot \frac{1 - e^{-z_m^2}}{z_m^2} - z_m + z_o \qquad z_m(0, z_o) = z_o \tag{6.17}$$

This is a nonlinear, ordinary differential equation for $z_m(t', z_o)$ for any fixed z_o. The initial position z_o may assume any value: $-\infty < z_o < \infty$. The temperature amplitude A_o is positive. For $A_o = 0$ we have the trivial solution $z_p(t') = z_o$.

The solution is rather straightforward. We have from (6.17):

$$dt' = \frac{dz_m}{A_o(1 - e^{-z_m^2})/(2z_m^2) - z_m + z_0} \tag{6.18}$$

We integrate from 0 to t'. On the right-hand side we get an integral from z_o to z_m. With s as integration variable we have:

$$t' = \int_{z_o}^{z_m} \frac{ds}{A_o(1 - e^{-s^2})/(2s^2) - s + z_o} \tag{6.19}$$

This is an explicit integral that gives t' as a function of z_m for any given z_o and A_o. It is easily calculated numerically. Figure 6.17 on pages 49-50 shows the result for $A_o = 1, 3, 10, 30$ and 100. These curves are to be compared with the previous ones that included the effect of P_c; Fig.6.13 for $A_o = 1$, Fig.6.11 for $A_o = 3$, Fig.6.14, upper right, for $A_o = 10$, Fig.6.15 for $A_o = 30$ and Fig.6.16 for $A_o = 100$. The character of the curves are remarkably similar. The differences are not too big. We can actually use this approximate, analytical solution in *assessments* of the maximal upward displacement.

6.4.2 Analysis of the integral for $z_m(t', z_o)$

Eq.(6.16) or (6.17) gives the velocity dz_m/dt' as a difference between the temperature component $v_{Tz}(0, z_m)$ and the counteracting weight $z_m - z_o$:

$$\frac{dz_m}{dt'} = \frac{A_o}{2} \cdot \frac{1 - e^{-z_m^2}}{z_m^2} - (z_m - z_o) \tag{6.20}$$

The situation is illustrated in Figure 6.18. The four full curves show the temperature component $v_{Tz}(0, z_m)$ for $A_o = 3$, 10, 20 and 30. Its maximum at $z_m = 0$ is $v_{Tz} = A_o/2$. The dashed sloping lines show $z_m - z_o$ for different start values z_o.

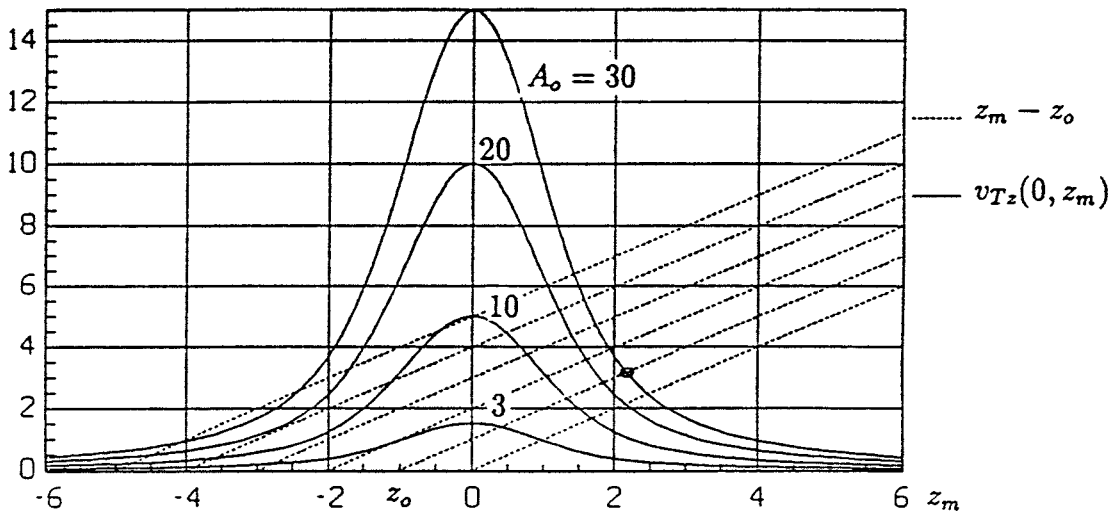

Figure 6.18. Figure to illustrate Eq.(6.20).

Consider as an example the case $z_o = -1$ and $A_o = 30$. The velocity of the particle is the difference between the curve v_{Tz} for $A_o = 30$ and $z_m - z_o = z_m + 1$. At $z_m = z_o = -1$ we get from the figure the velocity $9.5 - 0$. The velocity difference increases to $15 - 1$ at $z_m = 0$. Then the difference decreases, until it becomes zero at $z_m \simeq 2.14$. The denominator of (6.19) is then zero, and the point corresponds to $t' = \infty$.

For positive z_o, we have only one point where the two curves intersect and give the upper limit $z_m(\infty) = z'_{max}$. But for negative z_o we may have three zeros, for example for $z_o = -4$ and $A_o = 10$. This situation occurs for certain negative z_o, if the derivative of v_{Tz} with respect to z_o exceeds $+1$ at its inflexion point, which lies at $z_m = -0.8983$. The derivative at this point is:

$$z_m = -0.8983 \quad \Rightarrow \quad \frac{d}{dz_m}(v_{Tz}(0, z_m)) = \frac{A_o}{2} \cdot 0.53445 \tag{6.21}$$

We have the limit:

$$A_o = 3.742 \tag{6.22}$$

Above this limit there are three solutions for a certain interval of negative z_o-values. The lowest one is the one to use for z'_{max}. For $z_o = -4$ and $A_o = 10$, we get from the figure $z'_{max} \simeq -3.6$. When z_o is increased we reach a point, here $z_o \simeq -3.2$ for $A_o = 10$, where the first two solutions coalesce, and $z_m - z_o$ becomes a tangent to v_{T_z}. The end value z'_{max} makes a jump to the third solution for a positive value of z_m. This is the point of separation for the curves $z_m(t', z_o)$. In Figure 6.14 for $A_o = 10$, we see that this occurs for z_o between -3 and -1.5. From Figure 6.18 this occurs around $z_o = -3.3$. For $A_o = 3.0$, we get the separation for z_o between -4.5 and -3, while it occurs at $z_o \simeq -4.7$ in Figure 6.18. We see that the analytical results have a clear error here, but the character of process and the order of magnitude are certainly retained. The separation should not occur below the limit (6.22). This is consistent with our numerical results for $A_o = 3$ and smaller.

6.4.3 Final value $z'_{max}(z_o)$

The final point $z_m(\infty, z_o) = z'_{max}(z_o)$ is of particular interest. It is given by the points of intersection in Figure 6.18, where the two velocities in (6.20) balance each other. This equation may also be written in the form:

$$\frac{2}{A_o} \cdot (z_m - z_o) = \frac{1 - e^{-z_m^2}}{z_m^2} \qquad z_m = z'_{max}(z_o) \tag{6.23}$$

The situation is illustrated in Figure 6.19. The right-hand side, given by the upper full curve, intersects the straight line with the slope $2/A_o$ at $z_m = z'_{max}$. We see again the possibility of three solutions, in which case the lowest value is valid here.

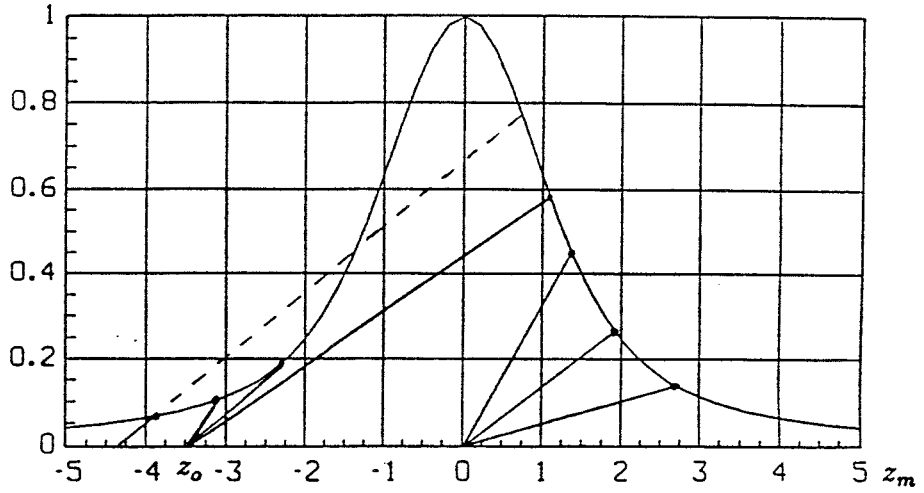

Figure 6.19. Figure to illustrate Eq.(6.23) to determine z'_{max} for given z_o and A_o.

The values of $z'_{max}(z_o)$ from Eq.(6.23) have been calculated for a number of A_o. The result is given in Table 6.2.

	$A_o = 0.1$	0.3	1	3	10	30	100	300
$z_o = -2.0$	-1.99	-1.96	-1.86	-1.22	1.04	1.93	3.12	4.72
-1.5	-1.48	-1.44	-1.25	0	1.19	2.04	3.25	4.86
-1.0	-0.97	-0.90	-0.57	0.39	1.34	2.17	3.38	5.00
-0.5	-0.46	-0.36	0	0.69	1.50	2.31	3.53	5.15
0	0.05	0.15	0.45	0.97	1.68	2.46	3.68	5.31
0.5	0.54	0.63	0.86	1.26	1.88	2.64	3.86	5.49
1.0	1.03	1.09	1.25	1.56	2.11	2.85	4.05	5.67
1.5	1.52	1.56	1.67	1.90	2.38	3.08	4.26	5.86
2.0	2.01	2.04	2.11	2.29	2.69	3.34	4.49	6.07

Table 6.2. Analytical, approximate values of $z'_{max}(z_o)$ for different A_o.

It is convenient to have explicit expressions for $z'_{max}(z_o)$. Formulas for $z_o \geq 0$, which are sufficiently accurate for our purposes, may be derived in the following way. Equation (6.23) is to be solved. The problem is the right-hand member, for which we introduce the following approximations:

$$\frac{1 - e^{-z_m^2}}{z_m^2} \simeq \begin{cases} 1 & 0 \leq z_m \leq 0.3 \\ 1.15 - z_m/2 & 0.3 \leq z_m < 1.5 \\ 1/z_m^2 & z_m \geq 1.5 \end{cases} \tag{6.24}$$

From this we get, when the solution of (6.23) falls in the first interval $0 < z_m \leq 0.3$:

$$z'_{max}(z_o) \simeq z_o + \frac{A_o}{2} \qquad 0 < A_o \leq 2(0.3 - z_o) \tag{6.25}$$

For the second interval $0.3 \leq z_m < 1.5$ we get:

$$z'_{max}(z_o) \simeq \frac{2.3A_o + 4z_o}{A_o + 4} \qquad 2(0.3 - z_o) \leq A_o \leq 5(1.5 - z_o) \tag{6.26}$$

In the third interval $z_m \geq 1.5$, we get a cubic equation:

$$z_m^2(z_m - z_o) = \frac{A_o}{2} \tag{6.27}$$

The solution for $z_o = 0$ is

$$z'_{max}(0) \simeq \sqrt[3]{A_o/2} \qquad A_o > 6.75 \tag{6.28}$$

There is a complicated but well-known solution to cubic equations. We get for $z_o > 0$:

$$z'_{max}(z_o) \simeq \frac{z_o}{3} + \frac{2z_o}{3} \cdot \cosh\left[\frac{1}{3}\text{arccosh}\left(1 + \frac{27A_o}{4z_o^3}\right)\right] \qquad A_o > 5(1.5 - z_o) \tag{6.29}$$

The formulas for $z_o = 0$ are of particular interest. We have from the above expressions:

$$z'_{max}(0) \simeq \begin{cases} A_o/2 & 0 < A_o \leq 0.6 \\ 2.3A_o/(A_o+4) & 0.6 \leq A_o < 7 \\ \sqrt[3]{A_o/2} & A_o \geq 7 \end{cases} \tag{6.30}$$

The expression for $A_o \geq 7$ lies above the other two approximations in the interval $0 < A_o \leq 7$. It may therefore be used as an *upper limit* for all A_o:

$$z'_{max}(0) \leq \sqrt[3]{A_o/2} \qquad A_o \geq 0 \tag{6.31}$$

For $z_o > 0$, we have from Eqs.(6.25), (6.26) and (6.29):

$$z'_{max}(z_o) \simeq \begin{cases} z_o + A_o/2 & 0 < A_o \leq 2(0.3 - z_o) \\ (2.3A_o + 4z_o)/(A_o+4) & 2(0.3 - z_o) \leq A_o \leq 5(1.5 - z_o) \\ z_o/3 + (2z_o/3) \cdot \cosh(p/3) & A_o > 5(1.5 - z_o) \\ p = \operatorname{arccosh}[1 + (27A_o)/(4z_o^3)] & \end{cases} \tag{6.32}$$

The different results for $z'_{max}(z_o)$ are compared in Table 6.3 for $z_o = 0, 1, -1$ for different A_o. The values obtained with the numerical model, row I, are given in Table 6.1. The values from the solution of (6.23), row II, are given in Table 6.2. Finally, row III shows the values from the above approximations for $z_o = 0$ (Eq.(6.30)) and $z_o = 1$ (Eq.(6.32)).

		$A_o = 0.3$	1	3	10	30	100
$z'_{max}(0)$	I	0.24	0.7	1.2	1.9	2.7	4.1
	II	0.15	0.45	0.97	1.7	2.5	3.7
	III	0.15	0.46	0.99	1.7	2.5	3.7
$z'_{max}(1)$	I	1.1	1.3	1.6	2.1	3.0	4.4
	II	1.1	1.3	1.6	2.1	2.8	4.1
	III	1.1	1.3	1.6	2.1	2.9	4.1
$z'_{max}(-1)$	I	-0.9	-0.3	0.9	1.6	2.4	4.0
	II	-0.9	-0.6	0.4	1.3	2.2	3.4

Table 6.3. Comparison of the largest upward displacement $z'_{max}(z_o)$.
I: Numerical calculations (Table 6.1),
II: Solution of Eq.(6.23) (Table 6.2),
III: Formulas (6.30) and (6.32).

We see that the approximate formulas (row III) are good approximations to the solution of Eq.(6.23) (row II). There are some difference between the numerical results with the model and the analytical expressions, but we can certainly use the latter ones for *assessments* of the largest upward displacement.

6.5 Formulas to assess upward displacement

A main endeavour in this study is to obtain formulas to *assess the largest upward displacement* of the groundwater, in particular for the water that starts at the center (0,0). We have seen that the largest displacements occur along the z'-axis.

The calculations above in this chapter are made in dimensionless form. Let $z_{max}(z_o)$ (m) denote the *real* maximum upward motion for a particle that starts at $(0, z_o)$ at $t' = 0$. Then we have from (6.3):

$$z_{max}(z_o) = \sqrt{4at_o} \cdot z'_{max}(z_o) \tag{6.33}$$

The dimensionless values $z'_{max}(z_o)$, calculated with the numerical model, are obtained from Figures 6.11-16 for $A_o = 3, 0.3, ..., 100$, respectively. The values for $z'_{max}(z_o)$ for $z_o = 0, 1, -1$ are also given in Table 6.1 for different A_o. Approximate analytical expression are given by Table 6.2, and Eqs.(6.30) and (6.32).

If we use formula (6.31) we have the estimate:

$$z_{max}(0) \simeq \sqrt{4at_o} \cdot \sqrt[3]{A_o/2}$$

or, inserting (6.5) for A_o,

$$z_{max}(0) \simeq \sqrt[3]{\frac{1}{2\pi\sqrt{\pi}} \cdot \frac{\alpha_T}{\alpha_c c_z^o C} \cdot \frac{E_o}{y_o} \cdot \frac{y_o}{\sqrt{4at_o}} e^{-y_o^2/(4at_o)}} \tag{6.34}$$

The time t_o, at which we take the point-source temperature field, may be chosen at will.

There is a maximum for $z_{max}(0)$ for a certain t_o. This maximum is determined by the last factor of (6.34), i.e. by the function:

$$g_1(\tau) = \frac{1}{\sqrt{\tau}} e^{-1/\tau} \qquad \tau = \frac{4at_o}{y_o^2} \tag{6.35}$$

A few values of g_1 are:

τ	0	0.1	0.25	0.5	1	1.5	2	2.5	3	5
$g_1(\tau)$	0	0.0001	0.04	0.19	0.37	0.42	0.43	0.42	0.41	0.37
$\sqrt[3]{g_1}$	0	0.05	0.33	0.58	0.72	0.75	0.75	0.75	0.75	0.72

τ	10	25	100	800	10000
$g_1(\tau)$	0.29	0.19	0.10	0.04	0.01
$\sqrt[3]{g_1}$	0.66	0.58	0.46	0.33	0.22

The quantity $\sqrt[3]{g_1}$ gives the variation of $z_{max}(0)$ with t_o. We see from the table that the maximum is very flat. The values lie between 0.33 and 0.75 for $0.25 < \tau < 100$. The maximum of g_1 is:

$$\frac{dg_1}{d\tau} = e^{-1/\tau} \cdot \left\{ -\frac{1}{2\tau\sqrt{\tau}} + \frac{1}{\sqrt{\tau}\tau^2} \right\} = 0 \quad \text{for} \quad \tau = 2 \tag{6.36}$$

$$g_{1,max} = g_1(2) = \frac{1}{\sqrt{2}} e^{-0.5} = 0.43 \tag{6.37}$$

This gives the largest $z_{max}(0)$ for variable t_o:

$$z_{max}(0)|_{max\, t_o} \simeq \frac{1}{\sqrt[6]{e}\sqrt{2\pi}} \cdot \sqrt[3]{\frac{\alpha_T}{\alpha_c c_z^o C} \cdot \frac{E_o}{y_o}} \qquad (y_o > \sqrt{4at_d}) \tag{6.38}$$

This formula is a *major result.* The distance y_o must exceed the limit (4.19). The maximum occurs for $t_o = y_o^2/(2a)$. The numerical factor is given by:

$$\frac{1}{\sqrt[6]{e}\sqrt{2\pi}} \simeq 0.34 \tag{6.39}$$

The *sensitivity* of $z_{max}(0)$, Eq.(6.38), for variations of the parameters is of great interest. The cubic root will diminish the sensitivity, since we have

$$\sqrt[3]{2} \simeq 1.26 \quad \sqrt[3]{10} = 2.2 \quad \sqrt[3]{100} = 4.6. \tag{6.40}$$

So, if α_T or c_z^o is changed by a factor 2, then $z_{max}(0)$ changes by the factor 1.26 only. If E_o or y_o are changed by a factor 10, then $z_{max}(0)$ changes by the factor 2.2 only. A change of E_o or y_o by a factor 100, will change $z_{max}(0)$ by a factor 4.6. Formula (6.38) gives the maximum with respect to t_o. The expression (6.34), valid for any t_o, declines as $1/\sqrt[6]{t_o}$. This means that $z_{max}(0)$ is extremely insensitive to changes of t_o after the initial period $0 < \tau < 2$ or $0 < t_o < y_o^2/(2a)$.

The above maximum concerns $z_{max}(0)$. The character of the flow field is determined by the value of A_o. Let us therefore also calculate the maximum of A_o for variable t_o. Expression (6.5) for A_o is written in the following way:

$$A_o = \frac{\alpha_T E_o}{\pi\sqrt{\pi}\alpha_c c_z^o C y_o^4} \cdot g_2(\tau)$$

$$g_2(\tau) = \frac{1}{\tau^2} e^{-1/\tau} \qquad \tau = \frac{4at_0}{y_o^2} \tag{6.41}$$

The function $g_2(\tau)$ gives the dependance on t_o. The maximum is:

$$\frac{dg_2}{d\tau} = e^{-1/\tau} \cdot \left(\frac{-2}{\tau^3} + \frac{1}{\tau^2} \cdot \frac{1}{\tau^2}\right) = 0 \quad \text{for} \quad \tau = 0.5 \tag{6.42}$$

$$g_{2,max} = g_2(0.5) = 4e^{-2} = 0.54 \tag{6.43}$$

A few values of $g_2(\tau)$ are:

τ	0	0.1	0.25	0.5	0.75	1	2.5	5	10	25	100
$g_2(\tau)$	0	0.005	0.29	0.54	0.47	0.37	0.11	0.03	0.01	0.002	0.0001
$\sqrt[3]{g_2}$	0	0.17	0.66	0.81	0.78	0.72	0.48	0.32	0.21	0.12	0.05

We see again that the variation with t_o has a very flat maximum. The factor $\sqrt[3]{g_2}$ lies between 0.21 and 0.81 for $0.11 < \tau < 10$. The largest value of the temperature amplitude A_o for variable t_o (y_o, E_o constant) is now:

$$A_o^{max} = \frac{4}{\pi\sqrt{\pi}e^2} \cdot \frac{\alpha_T}{\alpha_c c_z^o C} \cdot \frac{E_o}{y_o^4} \quad \text{for} \quad t_o = \frac{y_o^2}{8a} \tag{6.44}$$

The corresponding $z_{max}(0)$ becomes from (6.28) and (6.33), inserting $4at_o = y_o^2/2$:

$$z_{max}(0) = \frac{y_o}{2} \cdot \sqrt[3]{A_o^{max}} \tag{6.45}$$

or

$$z_{max}(0)|_{max\ A_o} = \sqrt[3]{\frac{1}{2\pi\sqrt{\pi}e^2}} \cdot \sqrt[3]{\frac{\alpha_T}{\alpha_c c_z^o C} \cdot \frac{E_o}{y_o}} \tag{6.46}$$

Here, the numerical factor is given by:

$$\sqrt[3]{\frac{1}{2\pi\sqrt{\pi}e^2}} \simeq 0.23 \tag{6.47}$$

6.6 Results for SKB repository

At long last, we are now able to *assess* the largest upward groundwater movement for a nuclear repository deep down in rock. The SKB system is described in Juhlin and Sandstedt (1989).

The heat release from a canister has the initial value $Q_{o,can}$ (W), and it decays with two exponential components with decay times t_d and t_{d1}:

$$Q_{can}(t) = Q_{o,can}\left[\alpha_1 e^{-t/t_d} + (1-\alpha_1)e^{-t/t_{d1}}\right] \tag{6.48}$$

The heat release up to a time t becomes:

$$E_{can}(t) = \int_0^t Q_{can}(t')dt' \tag{6.49}$$

$$E_{can}(\infty) = Q_{o,can}[\alpha_1 t_d + (1-\alpha_1)t_{d1}] \tag{6.50}$$

The total heat release from N_{can} canisters is then:

$$E_o = N_{can} \cdot E_{can}(\infty) \tag{6.51}$$

We use the following data:

$$Q_{o,can} = 533 \text{ W} \qquad t_d = 46 \text{ years} \qquad t_{d1} = 780 \text{ years}$$

$$\alpha_1 = 0.75 \qquad N_{can} = 300 \tag{6.52}$$

The total released heat is then:

$$E_o = 300 \cdot 533 \cdot (0.75 \cdot 46 + 0.25 \cdot 780) \cdot 3600 \cdot 24 \cdot 365 = 1.16 \cdot 10^{15} \text{ J} = 0.32 \text{ TWh} \tag{6.53}$$

We use the data of reference case (3.55). We have:

$$\frac{\alpha_T}{\alpha_c c_z^o C} = \frac{2 \cdot 10^{-4}}{0.72 \cdot 2 \cdot 10^{-5} \cdot 2.16 \cdot 10^6} = 6.43 \cdot 10^{-6} \text{ m}^4/\text{J} \tag{6.54}$$

The distance y_o from the canisters to the flow plane is an important parameter. We take a value close to the lower limit (4.19):

$$y_o = 100 \text{ m} \qquad (\sqrt{4at_d} = 97 \text{ m}) \tag{6.55}$$

Then we have according to (6.38):

$$z_{max}(0)|_{max\ t_o} \simeq 0.34 \cdot \sqrt[3]{6.43 \cdot 10^{-6} \cdot \frac{1.16 \cdot 10^{15}}{100}} = 143 \simeq 150 \text{ m} \tag{6.56}$$

The maximum occurs for the time:

$$t_o = \frac{y_o^2}{2a} = \frac{100^2}{2 \cdot 1.62 \cdot 10^{-6}} = 3.09 \cdot 10^9 \text{ s} = 98 \text{ years} \tag{6.57}$$

The Swedish nuclear program to year 2010 will require the storage of some 10 000 canisters. All these canisters cannot be placed in a small region, but let us hypothetically apply the main formula (6.38) for the heat release of all canisters. The heat E_o is increased by the factor 10 000/300, and we get: $z_{max}(0) = \sqrt[3]{33} \cdot 150 = 480$ m.

We assumed in the derivation of our formulas that all heat is released at a single point at the distance y_o from the flow plane. The case with canisters placed in a certain region should be investigated further. The distance y_o is then to be interpreted as some average distance to the flow plane. An extreme value of y_o (which does not satisfy (4.19)) is:

$$y_o = 10 \text{ m} \tag{6.58}$$

Then we get:

$$z_{max}(0)|_{max\ t_o} = 150 \cdot \sqrt[3]{10} = 320 \text{ m} \tag{6.59}$$

An example of a large y_o is:

$$y_o = 500 \text{ m} \quad \Rightarrow \quad z_{max}(0)|_{max\ t_o} = 150/\sqrt[3]{5} = 90 \text{ m} \tag{6.60}$$

The upward flow $z_{max}(0)$ is given by (6.34) for any t_o. The maximum $z_{max}(0) = 150$ m is obtained for $t_o \simeq 100$ years, which corresponds to $\tau = 2$. The value of $z_{max}(0)$ for other times t_o is given by the function $g_1(\tau)$, (6.35), and the table below the formula. We have for example:

$$t_o = 5 \text{ years}: \qquad \tau = 2 \cdot \frac{5}{100} = 0.1 \quad \sqrt[3]{g_1} = 0.05$$

$$z_{max}(0) = 150 \cdot \frac{0.05}{0.75} = 10 \text{ m} \tag{6.61}$$

We have in this way for a few t_o:

t_o (years)	5	25	100	500	5000
$z_{max}(0)$ (m)	10	120	150	130	90

We see that the sensitivity to the choice of t_o is quite small, except for the first period $t_o < 25$ years.

We have in the formulas and all considerations used the total released heat E_o. We may instead use the amount of heat released from $t = 0$ to $t = t_o$. Then we have in accordance with Eq.(6.49):

$$E_o \rightarrow E_o \left(1 - e^{-t_o/td}\right) \tag{6.62}$$

We get an extra factor for $z'_{max}(0)$ in (6.46). A few values are:

t_o/t_d	0.1	0.5	1	2	5
$\sqrt[3]{1 - e^{-t_o/t_d}}$	0.46	0.73	0.80	0.95	0.998

We see that this effect is rather small for $t_o > t_d$, and negligible for $t_o > 5t_d$

The above analysis is restricted to the case when the heat release from the canisters can be treated as an instantaneous point source. The distance y_o must exceed the limit (4.19). For smaller y_o, the temperature field must be represented in greater detail. This analysis is deferred to a coming study.

Chapter 7

Survey of results

There are two objectives for this study. The first one is to gain an understanding and insight into the coupled processes for heat, salt and groundwater. The second aim is to provide formulas and other tools of analysis to assess the largest upward motion from the heated region, in particular from the center (0,0), where the canisters may lie. This is a first study. Many questions, ideas and possibilities for further analyses remain to be explored.

A background to the problem is presented in Chapter 1. The general governing equations for water, salt and heat are discussed in Chapter 2. The convective heat flow can be neglected in the present application with very small groundwater flows. The thermal process is then governed by pure heat conduction and by the prescribed heat sources from the canisters. This leads to the important simplification that the thermal process is independent of the groundwater and salt process.

A major *assumption* is the use of Boussinesq's approximation with constant water viscosity μ_{wo} and constant water density ρ_{wo} except in the buoyancy term, for which the density $\rho_w(T, c)$ in linearized using a constant thermal expansion coefficient α_T and a corresponding coefficient α_c for the variation with salt concentration. Salt dispersion and diffusion are neglected. The third major assumption concerns the porous ground. In Chapter 2, the ground is treated as a homogeneous porous medium. In Chapter 3, and in the rest of the study, the water flow is assumed to be two-dimensional in a fracture plane $y = 0, -\infty < x < \infty, -\infty < z < \infty$. The process takes place far below the ground surface so that the upper boundary can be placed at infinity. The hydraulic conductivity of the plane is assumed to be constant. This is of course a drastic simplification of the real fracture system, but the behaviour for a single flow plane is judged to be the essential problem from which further analyses should be continued.

The undisturbed salt concentration $c_o(z)$ and water density increase downwards. A constant salt gradient c_z^o ($\mathrm{kg}_s/\mathrm{kg}_w\mathrm{m}$) is used. There is an undisturbed situation with a temperature $T_o(z)$ and a pressure $P_o(z)$. The deviations from equilibrium, or excess variables, for temperature, salt concentration and pressure are denoted T'', c'' and P'', respectively. The equations are given in a dimensionless form in Section 2.6 using scale factors L_1, $t_1 = t_c$, T_1, c_1 and P_1. The scale factor for the filtration velocity is denoted v_{f1}. The governing equations for the *dimensionless excess variables* become, (2.46-51):

$$(\nabla')^2 P' + \frac{\partial c'}{\partial z'} - \frac{\partial T'}{\partial z'} = 0 \tag{7.1}$$

$$\frac{\partial c'}{\partial t'} + \nabla' \cdot [(-z' + c')\vec{v}_f'] = 0 \tag{7.2}$$

$$\vec{v}_f' = -\nabla' P' - c'\hat{z} + T'\hat{z} \tag{7.3}$$

$$c'|_{t=0} = 0 \qquad T' \text{ given independently} \tag{7.4}$$

The first equation (7.1) determines the pressure P' due to the dimensionless excess density distribution $\rho' = c' - T'$. The third equation gives, according to Darcy's law, the filtration velocity with which the salt is moved convectively in accordance with equation (7.2). The dimensionless salt concentration, $\tilde{c} = -z' + c'$, contains an undisturbed part $-z'$, with unit gradient in the dimensionless formulation, and an excess part c'. The value of $\tilde{c}$ is constant for a salt-groundwater 'particle' when it moves around with the velocity field $\vec{v}_f'$. An important result, which is a consequence of the previous assumptions, is that the dimensionless equations (7.1-4) do not contain *any intrinsic parameters.* The only parameters to occur in our total process come from the scale factors and the parameters of the dimensionless temperature T'. Another important result of the dimensionless formulation is the scale factor for the time t_c ($t' = t/t_c$):

$$t_c = \frac{V_p \mu_{wo}}{k g \rho_{wo} \alpha_c c_z^o} \tag{7.5}$$

In the two-dimensional case, k/V_p is replaced by k^c/V_p^c, Eq.(3.4). This time gives a *characteristic time-scale* for flow induced by salt variations. It is noteworthy that t_c depends on salt parameters (α_c, c_z^o) and intrinsic permeability k, but it is independent of the thermal properties. The scale factor for length L_1 ($x' = x/L_1, ..$) is:

$$L_1 = \frac{\alpha_T T_1}{\alpha_c c_z^o} \tag{7.6}$$

This means that the length L_1 is chosen so that the water density change for the temperature change T_1 ($= \alpha_T T_1$) equals the density change over the height L_1 ($= L_1 \cdot \alpha_c c_z^o$) with a salt gradient c_z^o. The dimensionless excess density ρ' becomes with this choice equal to $c' - T'$, which expression occurs in (7.1) and (7.3).

In Chapter 3, the water flow is restricted to the plane $y = 0$. The thermal process is of course still three-dimensional, but only the temperatures in the plane $y = 0$ are used in our analysis. With our assumptions, we obtain explicit, analytical integrals for the pressure, Eq.(3.12), and flow field $\vec{v}_f$, Eq.(3.13), for any density distribution.

The water flow is driven by the density $\rho' = c' - T'$. We get, as described in Section 3.3, two components $\vec{v}_c$ and $\vec{v}_T$ for the water flow field.

The temperature field T' from a point heat source is rotationally symmetric in the flow plane $y = 0$. The contribution to the density, $-T'$, is a function of $r = \sqrt{x^2 + z^2}$ only, for any given time. In Section 3.2.2, explicit formulas for the pressure and flow for any density $\rho = \rho(r)$ are derived. This means that the temperature component $\vec{v}_T$ of the water flow field is obtained by *analytical* formulas. Only the salt component $\vec{v}_c$ is determined numerically.

The temperature fields from the heat sources at the canisters are discussed in Chapter 4. The solution for a point source, where the heat E_o (J) is released at $(0, y_o, 0)$ at $t' = 0$ is given. From this solution, the solution for a continuous heat source, (Q_o W)

and an exponentially decaying point source ($Q_o \cdot e^{-t/t_d}$ W) are derived by superposition. From these basic solutions, the temperature field for any distribution of canisters may be obtained by superposition.

The basic temperature field is actually the instantaneous point source, from which all other solutions are obtained by superposition. This initial study is confined to an analysis for this basic temperature field, which is reasonably accurate at the flow plane $y = 0$, if y_o exceeds the value $\sqrt{4at_d}$, Eq.(4.19). The case of smaller y_o is deferred to a coming study. The dimensionless temperature T' can then, at any particular time t_o, be written in the following way:

$$T' = A_o \cdot e^{-(r')^2} \tag{7.7}$$

The flow component $\vec{v}_T$ due to this temperature distribution is given by the explicit formulas (3.36). The dimensionless temperature amplitude A_o, Eq.(6.5), is proportional to E_o, and it depends on the chosen time t_o.

The characteristic time-scale t_c is estimated in Section 3.6. For our reference case (3.55) we get for a typical fracture width of 1 mm $t_c = 16.5$ hours, and for a width of 0.1 mm $t_c = 69$ days. The time-scale for the thermal process is from (3.61) of the order $t_T \simeq 50$ years. This means that we can consider the temperature field as virtually *time-constant* in the calculation of the salt flow process. We have to consider the salt flow process for the temperature field taken at any particular time t_o.

The flow process for the temperature field (7.7) has been determined by the numerical model for different values of A_o. The problem formulated in this way contains *one* dimensionless parameter only.

The numerical model is described in Chapter 5. This far, it has only been developed for the temperature flow $\vec{v}_T$ from a single, instantaneous point source. The numerical problem is solved for time-step after time-step. Consider an iteration step when the salt concentration c' is known. The ensuing flow component $\vec{v}_c$ is determined by a numerical evaluation of the explicit double integral (5.3). A particle-tracking technique is used. The particle (i, j) with a constant salt concentration $\tilde{c}_{ij} = -z_{ij} + c'_{ij}$ is displaced during the time-step in accordance with the total velocity $\vec{v}_T + \vec{v}_c$. We obtain the salt concentration at the next time-step.

The main problem in the model is to evaluate the double integral for $\vec{v}_c$, when c' is known numerically for the moving particles $(x_{ij}(t), z_{ij}(t))$. The integral is transformed from the (x', z')-plane to the $(x', \tilde{c})$-plane. This very particular method facilitates the calculations considerably. The double-sum is approximated by a Riemann sum based on the positions and salt concentrations of the particles.

Problems for the modelling technique are discussed in Section 6.3.3. The particles accumulate in certain areas and separate in others. This problem is solved by insertion and removal of particles. The $\tilde{c}$-curves may lie very close to each other in certain areas. A particle may then be removed, if two curves come too close to each other at a point. A particular problem is the spiraling of $\tilde{c}$-curves around the vortex points. See Figures 6.1-9. The particular numerical technique works quite well even for strongly spiraling, intertwined $\tilde{c}$-curves.

In Chapter 6, the results from calculations for $A_o = 0.3, 1, ...100$ are presented. There is a very clear barrier effect due to the salt gradient. The largest upward motion occurs on the z'-axis. Let $z'_{max}(z_o)$ denote the largest dimensionless upward displacement for the particle that starts at $(x', z') = (0, z_o)$ at $t' = 0$. We have according to Table 6.1 the

following results for different A_o:

A_o	0.3	1	3	10	30	100
$z'_{max}(0)$	0.24	0.7	1.2	1.9	2.7	4.1
$z'_{max}(1)$	1.1	1.3	1.6	2.1	3.0	4.4
$z'_{max}(-1)$	-0.9	-0.3	0.9	1.6	2.4	4.0

In Section 6.4, the upward motion is analysed under the assumption that the effect of the pressure P_c from the salt concentration can be neglected ($\vec{v}_c = -\nabla' P_c - c'\hat{z} \simeq -c'\hat{z}$). It is then possible to obtain an explicit integral, (6.19), for the motion along the z'-axis. Comparisons with the numerical results from the model (Figures 6.10-16 versus Figure 6.17) show that we obtain fairly good results even with this approximation. There are clear differences, but the analytical formulas can be used for *assessments* of the upward flow.

From the approximate analytical formulas, we derive in Section 6.4.3 explicit formulas for $z'_{max}(z_o)$ for $z_o = 0$ (Eq.6.30) and $z_o > 0$ (Eq.6.32). The comparison in Table 6.3 shows that these formulas can be used with sufficient accuracy for assessments of the largest upward flow $z'_{max}(z_o)$. We are in particular interested in $z'_{max}(0)$, i.e. the maximal upward displacement from $(0,0)$. We have from (6.30) and (6.31):

$$z'_{max}(0) \leq \sqrt[3]{A_o/2} \tag{7.8}$$

In Section 6.5, final formulas to assess the upward displacement are given. The largest upward displacement for a particle that starts from $(0, z_o \cdot L_1)$ (in real coordinates) is according to (6.3):

$$z_{max}(z_o) = L_1 \cdot z'_{max}(z_o) \qquad L_1 = \sqrt{4at_o} \tag{7.9}$$

The dimensionless displacement $z'_{max}(z_o)$ is given by the above Table 6.1 for different A_o and z_o.

For the most important case $z_o = 0$, we have from (7.8-9) the assessment, Eq.(6.34):

$$z_{max}(0) \simeq \sqrt{4at_o} \cdot \sqrt[3]{A_o/2} = \sqrt[3]{\frac{1}{2\pi\sqrt{\pi}} \cdot \frac{\alpha_T}{\alpha_c c_z^o C} \cdot \frac{E_o}{y_o} \cdot \frac{y_o}{\sqrt{4at_o}} \cdot e^{-y_o^2/(4at_o)}} \tag{7.10}$$

The time t_o is the time at which we take the temperature field from the point source. We can from (7.10) determine the largest $z_{max}(0)$ for different t_o. The maximum occurs for $4at_o = y_o^2/2$.

This maximum gives the following *final formula*, Eq.(6.38), to assess the upward motion:

$$z_{max}(0) = \frac{1}{\sqrt[6]{e}\sqrt{2\pi}} \cdot \sqrt[3]{\frac{\alpha_T}{\alpha_c c_z^o C} \cdot \frac{E_o}{y_o}} \qquad (y_o > \sqrt{4at_d}) \tag{7.11}$$

This is the largest upward displacement from $(0,0)$ for an instantaneous point source at any time. The numerical factor before the cubic root is equal to 0.34, Eq.(6.39).

Only the following six quantities occur in (7.11): The thermal expansion coefficient for water α_T, the corresponding coefficient for salt α_c (Eq.(2.30)), the salt concentration gradient c_z^o, the volumetric heat capacity of rock C, the total amount of released heat E_o, and the distance from the heat source to the flow plane y_o.

The intrinsic permeability k^c of the flow plane, or rather the flow resistance factor k^c/V_p^c in Darcy's equation (3.3), which is perhaps the most uncertain quantity of all, *does not occur* in formula (7.11). It occurs in t_c and influences the time-scale of the whole process. This gratifying independence is due to the fact that z_{max} is the result of a balance between upward thermal buoyancy and counteracting excess salt density.

The sensitivity of $z_{max}(0)$ for variations of the parameters is of great interest. The cubic root diminishes the sensitivity strongly, since we have: $\sqrt[3]{2} \simeq 1.26$ and $\sqrt[3]{10} \simeq 2.2$. So, if α_T (which we assumed constant) or c_z^o (which is somewhat uncertain) is changed by a factor 2, then $z_{max}(0)$ changes by the factor 1.26 only. The distance y_o from the flow plane is of course quite uncertain, but a change of y_o by a factor 10 will only change $z_{max}(0)$ by the factor 2.2. The other three quantities E_o, C and α_c are better known and less variable.

The formulas for z_{max} are based on the use of the temperature field from the heat release at any particular time t_o. It is shown in Section 6.5 that z_{max} is very insensitive to the choice of t_o, except for an initial, less critical period.

This study considers the largest upward flow starting with an undisturbed, perfectly stratified salt concentration $c_o(z)$. Any leakage would normally occur after quite a long time, at which time there is a quasi steady-state situation outside the local convection region. (The salt concentration distribution is strongly disturbed locally within the convection region.) But then the groundwater flow outside the convection region is smaller, and the upward displacement of contaminated groundwater from the canisters is expected to be no greater than the values obtained here.

Formula 7.11 is applied for the SKB repository concept in Section 6.6. Three hundred canisters, which corresponds to 1/33 of the storage requirements of the whole Swedish nuclear program to 2010, are considered. They release totally the heat $E_o = 0.32$ TWh. The data (3.55) and a distance $y_o = 100$ m give $z_{max}(0) \simeq 150$ m.

This study deals only with the temperature field from an instantaneous point source. The distance y_o should not be too small. A further study will remove this restriction and also deal with the case, when the canisters are distributed in a certain region, for example placed above each other in boreholes. The y_o-value used here is then to be interpreted as some average distance from the canisters to the flow plane. It seems reasonable that the distribution of canisters in the directions parallel to the flow plane will diminish the upward flow. The use of as much as 300 canisters in our example may then overestimate $z_{max}(0)$.

Nomenclature

$a = \lambda/C$	thermal diffusivity of the ground	(m^2/s)
A_o	dimensionless temperature amplitude, Eq. (6.5)	(-)
B	width of fracture zone	(m)
c	salt concentration	(kg_s/kg_w)
c'	dimensionless excess salt concentration	(-)
c''	excess salt concentration	(kg_s/kg_w)
$\tilde{c} = -z' + c'$	dimensionless total salt concentration	(-)
$c_o(z)$	undisturbed salt concentration	(kg_s/kg_w)
$c_o^z = -dc_o/dz$	salt concentration gradient	($kg_s/kg_w m$)
c_1	scale factor for salt concentration	(kg_s/kg_w)
C	volumetric heat capacity of the ground	(J/m^3K)
d	fracture width	(m)
E_{can}	total heat release from a canister	(J)
E_o	total heat release from the point source	(J)
f_ρ	radial density function, Eq. (3.25)	(-)
$g = 9.81$	standard gravity	(m/s^2)
h	heat source	(W/m^3)
k	intrinsic permeability	(m^2)
k^c	intrinsic permeability of fracture zone	(m^3)
L_1	scale factor for length coordinates	(m)
P	groundwater pressure	(Pa)
P'	dimensionless excess pressure	(-)
P''	excess pressure	(Pa)
P_1	scale factor for pressure	(Pa)
P_c, P_T	dimensionless salt and temperature components of the pressure	(-)
$\vec{q}_w = (q_{wx}, q_{wy}, q_{wz})$	volumetric groundwater flow	(m_w^3/m^2s)
$\vec{q}_w^c$	volumetric groundwater flow in fracture plane or fracture zone	(m_w^3/ms)
Q_o	rate of heat release	(W)
$Q_{o,can}$	initial rate of heat release from a canister	(W)
$r = \sqrt{x^2 + z^2}$	radial distance in flow plane	(m)
r'	dimensionless radial distance	(m)
r_1	radial length	(m)
t	time	(s)
t'	dimensionless time	(-)
t_o	time at which the temperature field is taken, see Section 6.1	(s)
t_c	characteristic time-scale, scale factor for time	(s)
t_d	decay time for heat source, Eq.(4.11)	(s)
t_T	characteristic time-scale for temperature field, Eq. (3.60)	(s)
T	temperature in the ground	(°C)

T'	dimensionless excess temperature	(-)
T''	excess temperature	(°C)
T_o	undisturbed ground temperature	(°C)
T_1	scale factor for temperature	(°C)
T^c	temperature in fracture plane	(°C)
T^c_{int}	integral of the temperature over the fracture plane, Eq. (4.3)	(m^2°C)
U	solution to Eq. (3.14)	(-)
$\vec{v}_f$	filtration velocity	(m/s)
$\vec{v}'_f$	dimensionless filtration velocity	(-)
v_{f1}	scale factor for filtration velocity	(m/s)
v_c, v_T	dimensionless salt and temperature components of filtration velocity	(-)
V_p	pore volume	(m^3_w/m^3)
V^c_p	pore volume of fracture zone	(m^3_w/m^2)
x, y	horizontal coordinates	(m)
x', y'	dimensionless horizontal coordinates	(-)
y_o	distance from heat source to flow plane	(m)
z	vertical coordinate	(m)
$\hat{z}$	vertical unit vector pointing upwards	(-)
z'	dimensionless vertical coordinate	(-)
$z_m(t', z_o)$	particle motion along the z'-axis	(-)
$z'_{max}(z_o)$	maximal dimensionless upward displacement	(-)
$z_{max}(z_o)$	maximal upward displacement	(m)
z_o	dimensionless starting point on the z'-axis	(-)
α_c	relative density increase with salt concentration, Eq. (2.30)	($1/(kg_s/kg_w)$)
α_T	thermal expansion coefficient, Eq.(2.30)	(1/°C)
λ	thermal conductivity of the ground	(W/mK)
μ_w	dynamic viscosity of water	(kg/ms)
ρ_w	density of water	(kg/m^3)
$\rho' = c' - T'$	dimensionless excess density	(-)
ρ''	excess water density, Eq. (2.26)	(kg/m^3)
ϕ_c	angle between the z-axis and fracture plane	(rad)
$\nabla = \left(\frac{\partial}{\partial x}, \frac{\partial}{\partial y}, \frac{\partial}{\partial z}\right)$	gradient operator	(m^{-1})
$\nabla' = \left(\frac{\partial}{\partial x'}, \frac{\partial}{\partial y'}, \frac{\partial}{\partial z'}\right)$	dimensionless gradient operator	(-)

Here, m^3_w denotes cubic meter of water, kg_s kilogram of dissolved salt and kg_w kilogram of water including the dissolved salt. The prime $'$, which denotes dimensionless excess variables, is sometimes suppressed for convenience. In particular, it should be noted that the following variables are *dimensionless*:

$$\tilde{c} \quad P_c \quad P_T \quad v_c \quad v_T \quad z_o \quad z_m(t', z_o)$$

References

Bear, J., 1972, Dynamics of Fluids in Porous Media, American Elsvier Publishing Company, New York.

Carslaw, H.S., Jaeger, J.C., 1959, Conduction of Heat in Solids, Oxford University Press.

Courant, R., Hilbert, D., 1968, Methoden der Mathematischen Physic, Springer-Verlag, Berlin.

CRC Handbook, 1971, Handbook of Chemistry and Physics, The Chemical Rubber Co, Ohio.

Hodgkinson, D.P.,1980, A Mathematical Model for Hygrothermal Convection around a Radioactive Waste Depository in Hard Rock, Annals of Nuclear Energy, Vol.7, pp 313-334, Pergamon Press.

Juhlin, C., Sandstedt, H., 1989, Storage of nuclear waste in very deep boreholes: Feasibility study and assessment of economic potential, Technical Report 89-39, Swedish Nuclear and Waste Management Co, Stockholm.

Schmidth, E., Grigull, U., 1979, Properties of water and stream in SI-units, Springer-Verlag, Berlin.

List of SKB reports

Annual Reports

1977-78
TR 121
KBS Technical Reports 1 – 120
Summaries
Stockholm, May 1979

1979
TR 79-28
The KBS Annual Report 1979
KBS Technical Reports 79-01 – 79-27
Summaries
Stockholm, March 1980

1980
TR 80-26
The KBS Annual Report 1980
KBS Technical Reports 80-01 – 80-25
Summaries
Stockholm, March 1981

1981
TR 81-17
The KBS Annual Report 1981
KBS Technical Reports 81-01 – 81-16
Summaries
Stockholm, April 1982

1982
TR 82-28
The KBS Annual Report 1982
KBS Technical Reports 82-01 – 82-27
Summaries
Stockholm, July 1983

1983
TR 83-77
The KBS Annual Report 1983
KBS Technical Reports 83-01 – 83-76
Summaries
Stockholm, June 1984

1984
TR 85-01
Annual Research and Development Report 1984
Including Summaries of Technical Reports Issued during 1984. (Technical Reports 84-01 – 84-19)
Stockholm, June 1985

1985
TR 85-20
Annual Research and Development Report 1985
Including Summaries of Technical Reports Issued during 1985. (Technical Reports 85-01 – 85-19)
Stockholm, May 1986

1986
TR 86-31
SKB Annual Report 1986
Including Summaries of Technical Reports Issued during 1986
Stockholm, May 1987

1987
TR 87-33
SKB Annual Report 1987
Including Summaries of Technical Reports Issued during 1987
Stockholm, May 1988

1988
TR 88-32
SKB Annual Report 1988
Including Summaries of Technical Reports Issued during 1988
Stockholm, May 1989

1989
TR 89-40
SKB Annual Report 1989
Including Summaries of Technical Reports Issued during 1989
Stockholm, May 1990

1990
TR 90-46
SKB Annual Report 1990
Including Summaries of Technical Reports Issued during 1990
Stockholm, May 1991

1991
TR 91-64
SKB Annual Report 1991
Including Summaries of Technical Reports Issued during 1991
Stockholm, April 1992

Technical Reports

List of SKB Technical Reports 1992

TR 92-01
GEOTAB. Overview
Ebbe Eriksson[1], Bertil Johansson[2], Margareta Gerlach[3], Stefan Magnusson[2], Ann-Chatrin Nilsson[4], Stefan Sehlstedt[3], Tomas Stark[1]
[1]SGAB, [2]ERGODATA AB, [3]MRM Konsult AB
[4]KTH
January 1992

TR 92-02

Sternö study site. Scope of activities and main results

Kaj Ahlbom[1], Jan-Erik Andersson[2], Rune Nordqvist[2], Christer Ljunggren[3], Sven Tirén[2], Clifford Voss[4]
[1]Conterra AB, [2]Geosigma AB, [3]Renco AB, [4]U.S. Geological Survey

January 1992

TR 92-03

Numerical groundwater flow calculations at the Finnsjön study site – extended regional area

Björn Lindbom, Anders Boghammar
Kemakta Consultants Co, Stockholm

March 1992

TR 92-04

Low temperature creep of copper intended for nuclear waste containers

P J Henderson, J-O Österberg, B Ivarsson
Swedish Institute for Metals Research, Stockholm

March 1992